NEAR-EARTH OBJECT (NEO) ANALYSIS OF TRANSPONDER TRACKING AND GRAVITY TRACTOR PERFORMANCE

Submitted to B612 Foundation

Final Report

JPL Task Plan No. 82-120022

September 22, 2008

Study carried out and report written by D.K. Yeomans, S. Bhaskaran, S.B. Broschart, S.R. Chesley, P.W. Chodas, M.A. Jones, and T.H. Sweetser

Intended for use by the B612 Foundation. May contain Caltech/JPL proprietary information and be subject to export control; comply with all applicable U.S. export regulations.

Table of Contents

1 SCIENTIFIC/TECHNICAL WORK 1-0
1.1 Introduction 1-0
1.2 Objectives 1-1
1.2.1 Study Objectives 1-1
1.3 Technical Approach and Methodology 1-2
1.4 Work Plan 1-2
1.4.1 Statement of Work and Results 1-2
1.4.2 Subtask 1 Results 1-3
1.4.3 Subtask 2 Results 1-17
1.4.4 Subtask 3 Results 1-48
1.4.5 Subtask 4 Results 1-55
1.4.6 Subtask 5 Results 1-55
1.4.7 Key Milestones and Products 1-55
1.5 Study Conclusions 1-56
2 REFERENCES 2-59

May contain Caltech/JPL proprietary information and be subject to export control; comply with all applicable U.S. export regulations.

1 Scientific/Technical Work

1.1 Introduction

This report is submitted to the B612 Foundation as part of JPL Task Plan Number 82-120022. The report outlines the tasks originally planned in the proposal as well as the work that was actually performed, the conclusions, and the plan for possible future work.

Lu and Love (2005) outlined a gravity tractor concept in which the gravitational attraction between an Earth-threatening asteroid and a nearby thrusting spacecraft could be used to slightly adjust the motion of the asteroid years before the potential collision. Although the very small acceleration imparted to the asteroid by the gravity tractor would most likely be insufficient for most primary deflection attempts, the gravity tractor could be used to slightly alter or trim the motion of the asteroid following a deflection attempt by another technique (e.g., a kinetic energy impact by a colliding spacecraft), should the primary deflection attempt inadvertently push the asteroid through a "keyhole" into a resonant return trajectory that would lead to a subsequent Earth impact. A keyhole is defined on the target plane (also called the b-plane), which is the plane perpendicular to the incoming asymptote of an asteroid's trajectory during a close approach to a planet. The Earth close approach can perturb an asteroid's trajectory onto a path that brings it back to an Earth impact an integral number of years later. A "keyhole" is the small region in the target plane that leads to a perturbed trajectory, impacting during a subsequent close approach. The target plane of a close approach can have numerous such keyholes.

The work outlined in this study addresses the scenario in which a near-Earth object (NEO) is on a possible collision course with the Earth and a gravity tractor spacecraft carrying a radio transponder (t-GT) is dispatched to rendezvous with the object. The mission's first objective would be to verify the possible impact via precision tracking of the spacecraft. If the NEO is confirmed to be on a collision course and the impulse required to avoid collision is beyond the capability of the gravity tractor, another deflection technique (such as a kinetic impactor) would be employed to effect a primary deflection. After the deflection, the t-GT would be used to precisely determine the new trajectory of the NEO, and it would be available (if necessary) to slightly alter or trim the NEO's motion to ensure it is not headed for a near-term resonant return (keyhole) and a resulting secondary Earth impact trajectory.

The objectives of this study were to analyze the two primary capabilities of the t-GT spacecraft in the above scenario. First, we examined the spacecraft requirements for accurately determining the trajectory of the NEO, both before and after a deflection. This is the "transponder" part of the t-GT mission, which would be used both to verify that the primary deflection successfully averted the primary impact and to determine whether the NEO might pass through a keyhole. Secondly, we studied the requirements for the "gravity tractor" portion of the mission, which is the capability of "towing" the NEO trajectory so that it passes sufficiently far away from a keyhole.

There were 5 subtasks identified in the original proposal and this report is organized in order of these subtasks:

1. Select a strawman NEO orbit and a timeline for the case study.

May contain Caltech/JPL proprietary information and be subject to export control; comply with all applicable U.S. export regulations.

   a. Select a hypothetical Earth impactor "2016 NM4" with an impact in 2049.
   b. Analyze the orbit of 2016 NM4 and its Earth and Venus close approaches.
   c. Simulate a primary kinetic impactor deflection in 2028 to avoid the 2049 impact.
   d. Analyze the "keyholes" in the 2049 Earth target plane.
   e. Simulate an inadvertent deflection into the 6:5 keyhole in the 2049 Earth target plane – leading to potential impact in 2054.
   f. Simulate gravity tractor operations beginning in July 2032 and lasting ~200 days.
2. Study the gravity tractor spacecraft requirements to accelerate a NEO in a pre-determined direction and quantity.
   a. Select a representative NEO physical model (i.e., 2016 NM4 is a scaled down Itokawa shape model)
   b. Demonstrate that a spacecraft control law is possible so that it can thrust and hover closely in front of an irregularly shaped, rotating asteroid.
3. Study NEO tracking using radiometric tracking of the nearby spacecraft:
   a. How accurately can the pre-deflection orbit of 2016 NM4 be determined?
   b. Following the primary deflection via kinetic impactor, how long an interval of spacecraft tracking does it take to determine the resultant change in velocity (ΔV) on the asteroid to sufficient accuracy?
   c. Following the gravity tractor phase, how long an interval of spacecraft tracking does it take to determine the acceleration imparted to the asteroid to sufficient accuracy?
4. Perform preliminary analysis of a mission design and implementation. (Work on Subtask 4 was descoped because the customer did not wish to pursue the Team X study at this time.)
5. Perform Team X study to develop full mission concept design and cost estimates (descoped).

1.2 Objectives

1.2.1 Study Objectives

The overarching objectives of this study were to determine the feasibility of using the gravity tractor concept for use in NEO impact mitigation and to build credibility for the concept, assuming it is concluded to be viable. In order to gain insight into the feasibility of the gravity tractor concept, the following two focus areas were addressed by the Guidance, Navigation and Control team at JPL:

1. Determine the performance characteristics of the gravity tractor as a function of NEO proximity and provide control guidelines for station keeping and navigation in close proximity to an irregularly-shaped, rotating NEO, such that the spacecraft can change the trajectory of the NEO into a non-threatening trajectory without jeopardizing the spacecraft's safety.

May contain Caltech/JPL proprietary information and be subject to export control; comply with all applicable U.S. export regulations.

2. Determine whether radio tracking of the transponder/gravity tractor spacecraft could improve the trajectory of the NEO sufficiently to ensure that the NEO would not enter a keyhole within a specified degree of uncertainty and interval of time.

Building the credibility of the concept was begun by demonstrating its viability through attaining positive results from the models used to study the focus areas noted above. Additional enhancement of the concept's integrity could be achieved if the customer chose to pursue this option or some variation of this option, through a Team X study that would

3. Develop a rough full mission concept and design.
4. Obtain a cost estimate for the mission concept.

1.3 Technical Approach and Methodology

The approach taken for this study involved breaking up the objectives into two sections: (1) concept feasibility; and (2) credibility of the implementation concept. A team from JPL's Guidance Navigation and Control (GNC) group was formed to address the feasibility issues of station keeping and navigation near a small body and accurately tracking a NEO with a transponder. Various models were used to address each of the subtasks noted in the statement of work (section 1.4.1). Results from each of these subtasks directly address objectives 1 and 2 above. The option of providing additional details to increase the credibility of the implementation concept was also added as subtask 4. If desired, the customer could choose one of the two Team X study options at the end of this study.

1.4 Work Plan

1.4.1 Statement of Work and Results

Demonstration of Concept Feasibility

Work outlined in Subtasks 1-3 of the original proposal focused upon demonstrating feasibility of the concept and directly addresses objectives: (1) station keeping and navigation at the NEO; and (2) tracking accuracy enabled by the transponder. This work was completed over a seven month time period from the start of the contract by the JPL GNC team.

Subtask 1: Selection of a strawman NEO, orbit, and timeline for case study.

A strawman target NEO was selected with the following characteristics:

- V_∞ with respect to Earth in the range: 5-10 km/s
- Effective diameter: 140 m
- Bulk density: 2.0 g/cm^3
- Axial ratios: 1:1:2
- Rotation period: 12 hr
- Rotation pole obliquity: 45°

May contain Caltech/JPL proprietary information and be subject to export control; comply with all applicable U.S. export regulations.

- Size and spin state may be varied parametrically for a portion of the study

The existing Itokawa shape model (pre-Hayabusa) was scaled to the desired effective diameter for use in the analysis outlined in subtask 2. It should be noted that the selected target's obliquity and rotation period used in our analysis (135 degrees and 6 hours) differ from what was proposed (45 degrees, 12 hours). See Table 2 for more details about the selected target's properties.

1.4.2 Subtask 1 Results

Target Selection Results: Virtual Impactor 2016 NM4

The hypothetical asteroid, provisionally designated 2016 NM4 (Chesley and Chodas, 2008), is discovered in July 2016, shortly after the initiation of the Large Synoptic Survey Telescope (LSST) survey, and is headed for a collision with Earth 33 years later, in September 2049. The primary impact location, chosen at random, is in the South Pacific, about 5400 km due south of Los Angeles and 1500 km NW of Easter Island (Figure 1).

Figure 1. Impact location for 2016 NM4 on 2049 Sept. 12.

The asteroid is an Aten-class object on what we believe is a rather typical impactor trajectory, a low-inclination, shallow-crossing orbit largely interior to Earth. Figure 2 shows the orbit of the asteroid along with the orbits of Earth and Venus. The hazardous close approaches with the Earth occur at the asteroid's descending node, indicated on the Figure. Figure 3 shows the motion of the asteroid in a frame rotating with the Earth. Because the object is very near the 13:10 mean motion resonance with Earth, its orbit path in Figure 3 comes very close to repeating after 10 years (13 revolutions of the asteroid). It therefore has particularly good observing circumstances every 10 years starting with the 2016 discovery apparition. In addition, since the

May contain Caltech/JPL proprietary information and be subject to export control; comply with all applicable U.S. export regulations.

orbit is also fairly close to the 4:3 resonance, the asteroid can be observed three years before and after the favorable apparitions, when it passes through the lobes above and below the Earth in Figure 3. Table 1 details the planetary close approaches within 0.1 AU for 2016 NM4 from the time of discovery through impact. We note the Earth close approach in 2046, three years prior to the primary impact. This encounter has a minimum distance of about one lunar distance, and leads to a 100-fold separation of nearby trajectories between 2046 and 2049. As a result, the 2046 encounter provides improved leverage for the deflection effort, at the expense of a similar increase in prediction uncertainty in 2049, the ramifications of which are discussed later.

The dynamical model used in these orbit calculations includes a standard set of perturbations, including the gravitational accelerations of the Sun, Moon, 8 planets and 4 asteroids, along with the effects of solar relativity. A more complete dynamical model, including for example the Yarkovsky effect, would be adopted as needed.

Table 1. Planetary and lunar close approaches (within 0.1 AU) of 2016 NM4 from discovery through impact. The last line represents the impact, since the close approach distance is less than the radius of the Earth.

Date	Body	Dist.(AU)
2016 Aug 27.94383	Earth	0.042706
2017 Oct 30.31594	Venus	0.080965
2020 Dec 5.38243	Venus	0.062307
2024 Jan 7.88372	Venus	0.046527
2026 Aug 15.82433	Earth	0.055507
2027 Feb 5.14327	Venus	0.042289
2030 Mar 5.01357	Venus	0.040493
2033 Mar 29.28549	Venus	0.052710
2036 Apr 17.59255	Venus	0.073968
2036 Aug 31.82278	Earth	0.033996
2039 May 11.61451	Venus	0.081424
2042 Jun 4.36096	Venus	0.087426
2045 Jun 26.60054	Venus	0.094500
2046 Sep 13.67208	Earth	0.002772
2049 Sep 11.98767	Moon	0.001902
2049 Sep 12.35720	Earth	0.000019

While simulations show that most impactor discoveries surpass 99% impact probability very early in their second apparition, 2016 NM4 does not reach that threshold until the fourth apparition, fully ten years after discovery. By the end of the discovery apparition the impact probability has reached only 0.2%. Three years later it is recovered and the impact probability shoots to 10%, topping 48% by the end of the apparition in Nov. 2019. It is re-observed in 2023 and reaches 85% probability by the end of that observing window. It finally exceeds 99% at the outset of the fourth apparition, in 2026. This somewhat slow rise in impact probability for 2016 NM4 is due to the poor observing circumstances (low solar elongations and large geocentric distances) encountered during the second and third apparitions, as well as the presence of a 1.1 lunar distance encounter in 2046, which amplifies orbit uncertainties three years prior to impact.

May contain Caltech/JPL proprietary information and be subject to export control; comply with all applicable U.S. export regulations.

Note that the impact probabilities stated here neglect the possibility of radar measurements, despite the fact that radar observations would very likely be made in late August 2016, when the Arecibo SNR is of order 10^3 and the impact odds would be around 1 in 2500. See Figure 4 for a graph showing the rise of computed impact probability of the asteroid. While we have not considered radar astrometry in 2016, it is likely that the impact probability would exceed 99% by 2023, or even 2019, if they were included.

We note there is some discrepancy between the assumed albedo (0.143) and the assumed bulk density (2 g/cm^3). This is because, based on our limited current understanding, smaller objects with relatively high albedos (0.1-0.2) have somewhat higher densities, in the 2.5-3.5 g/cm^3 range, whereas darker asteroids tend to have lower densities. This is not a particularly severe contradiction, nor is it a critical concern for the study, but it could easily be resolved by assuming a fairly high macro-porosity, which is entirely consistent with the rather long rotation period. Alternatively, reducing the albedo to a number more consistent with the assumed density (say 0.06) and increasing the absolute magnitude to 23 would also lead to reasonable parameter values. None of this affects the mass or size of the target asteroid and is therefore of no importance to the outcome of this study.

Table 2 lists most of the relevant impact, orbital, and physical parameters for our target asteroid 2016 NM4

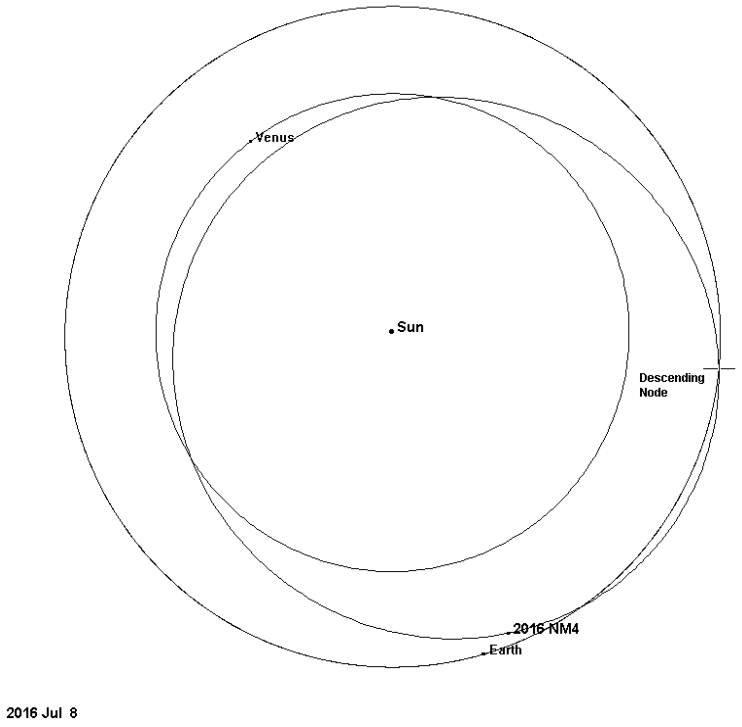

Figure 2. Orbits of Earth, Venus and 2016 NM4. The positions are noted for the July 2016 discovery of 2016 NM4.

May contain Caltech/JPL proprietary information and be subject to export control; comply with all applicable U.S. export regulations.

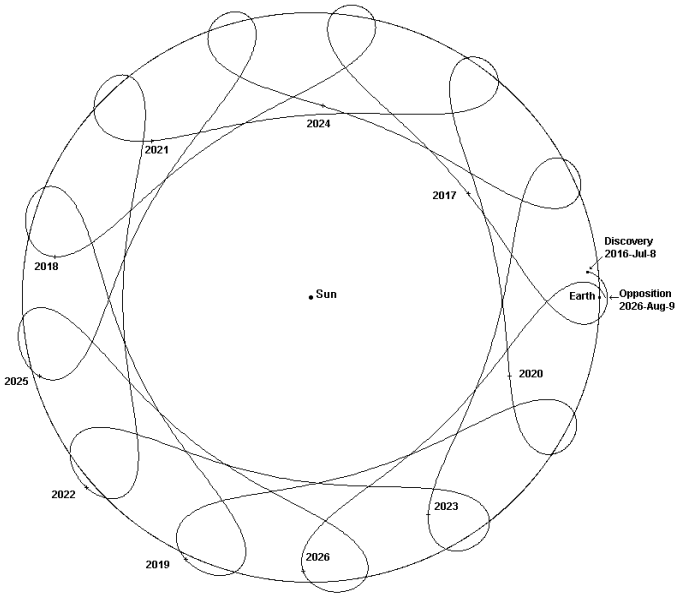

Figure 3. Orbit of 2016 NM4 relative to Earth in the Earth rotating frame.

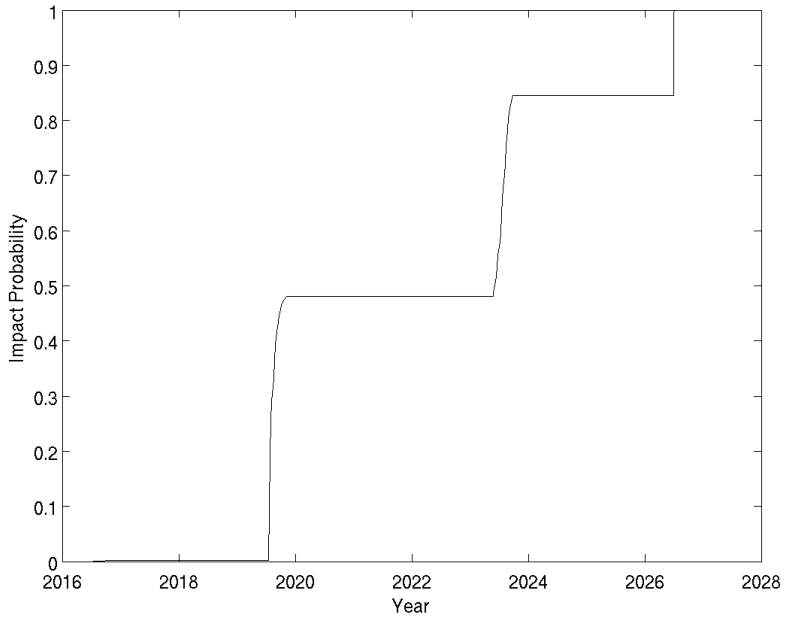

Figure 4. Rise of computed impact probability for 2016 NM4 from discovery in July 2016 through 2028.

May contain Caltech/JPL proprietary information and be subject to export control; comply with all applicable U.S. export regulations.

Table 2. Relevant Parameters for Asteroid 2016 NM4.

Discovery Date	July 8, 2016
Earth Impact information	
Date	2049-09-12.35
Location	269.233º E, -14.514º S
Velocity	12.3 km/s
Orbital Properties	
Orbital Period	280.756 day (0.7687 yr)
Eccentricity	0.2490
Inclination	5.185º
Perihelion dist.	0.6198 AU
Semi-major axis	0.8254 AU
Aphelion dist.	1.0309 AU
V_∞ S/C impact velocity	5.1 km/s
Physical Properties	
Absolute Magnitude	22.0
Albedo	14.3%
Effective radius[1]	70 m
Shape	Scaled Itokawa radar model[2]
Bulk density	2.0 g/cm^3
Mass	2.868×10^9 kg
GM	1.914×10^{-10} km^3/s^2
Obliquity	135º
Rotation period	6 hours
Spin axis orientation	$(\alpha,\delta) = (121º, -29.3º)$
	$(\lambda,\beta) = (132.4º, -48.3º)$

Deflection Scenario Timeline

By the end of 2023 the impact probability would have risen to about 85% using only optical observations and, with the incorporation of radar observations, probably in excess of 99%. Therefore we assume that the decision would be taken at that time to launch both a rendezvous t-

[1] Radius of sphere of equivalent volume
[2] See Ostro et al. (2005).

May contain Caltech/JPL proprietary information and be subject to export control; comply with all applicable U.S. export regulations.

GT and a kinetic energy Impactor Deflection Mission (IDM). We assume both missions would be launched on the same booster in mid-2026 around the time of the asteroid's close Earth approach, which provides for a particularly favorable opportunity for a quick rendezvous. Thus the t-GT spacecraft should be on station only months after launch, by December 2026, and we assume the IDM spacecraft takes two additional years to gain orbital energy for a higher velocity impact that takes place on July 4, 2028, a few weeks before the asteroid's perihelion passage. Gravity tractor operations would start in July 2032 to trim the trajectory in order to avoid a secondary impact after 2049. This "tractoring" phase would be expected to take several months.

Impactor Deflection

The IDM would collide with 2016 NM4 with a relative velocity of about 5 km/s. The mission design for the IDM is beyond the scope of the present study; we simply assume that the spacecraft would be maneuvered in order to effect the desired collision. The orbit of the concept is shown in Figure 5. The spacecraft would follow an exterior tangential orbit at the point of collision, so that the impact would result in a purely along-track increase in asteroid velocity (positive ΔV). This constrains the IDM spacecraft orbit to that given in Table 3:

Table 3. IDM Spacecraft Orbit Constraints.

Eccentricity	0.5329
Perihelion dist.	0.6545 AU
Semi major axis	1.401 AU
Aphelion dist.	2.148 AU
Perihelion date	2028 Jul 13.28669
Long. Asc. Node	170.379º
Arg. Perihelion	316.555º
Inclination	5.429º
Period	1.659 yr

The deflection imparted by the IDM is given by:

$$\Delta V = \beta \, (m/M) \, V_\infty$$

where m is the spacecraft mass, M is the asteroid mass, V_∞ is the spacecraft relative velocity at impact, and β is the momentum enhancement factor. For $\beta = 1$, we have a plastic collision, with the impactor absorbed into the body without producing ejecta. For $\beta = 2$, the collision is elastic, with the ejecta momentum equal and opposite to the impactor momentum. Super-elastic collisions ($\beta > 2$) are considered likely, and sub-plastic collisions ($\beta < 1$), where the material spalled from the back of the asteroid carries more momentum than that of the crater ejecta, are considered very unlikely. We assume here that $1 < \beta < 5$, and that, nominally, $\beta = 2$.

May contain Caltech/JPL proprietary information and be subject to export control; comply with all applicable U.S. export regulations.

We assume an IDM mass of 1150 kg at impact, which leads to a $\Delta V/\beta = 2$ mm/s. The nominal momentum enhancement of $\beta = 2$ produces $\Delta V = 4$ mm/s, while the full range of β values produces deflections in the range 2-10 mm/s. This range of deflections produces a range of miss distances in 2049 of 4.7-30.3 $R_\oplus$, with a nominal value of 11.0 $R_\oplus$.

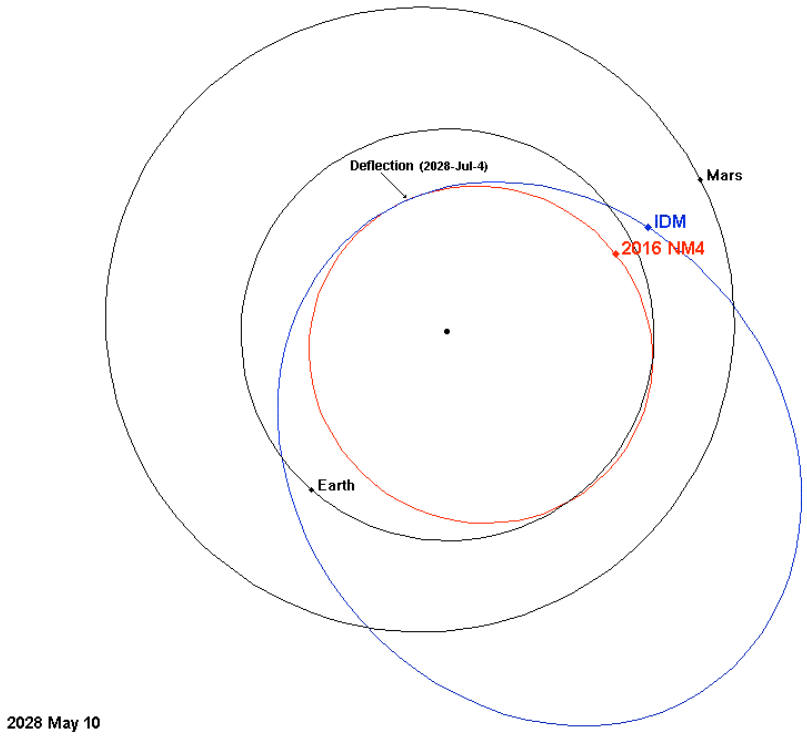

Figure 5. Orbit of Impactor Deflection Mission (IDM) spacecraft (in blue) and asteroid 2016 NM4 (in red), as well as the orbits of Earth and Mars. The positions of the objects two months before the primary deflection are also shown, along with the location of the primary deflection.

For the purposes of this study, we assume that the asteroid is successfully deflected away from the 2049 impact, but happens to be deflected onto a new impact trajectory, with the secondary collision occurring sometime within ten years after the date of the 2049 primary impact. There are a number of resonances available for this scenario, and we select the 6:5 resonance, with an orbital period of 0.8333 yr, corresponding to an impact in September 2054. This secondary impact is obtained for a near-nominal IDM deflection of $\Delta V = 4.6889 \pm 0.00015$ mm/s, which implies a very realistic $\beta = 2.34$. A list of these secondary impact possibilities is given in Table 4. Note that a one-year return to impact is possible for the unlikely case of a sub-plastic collision.

May contain Caltech/JPL proprietary information and be subject to export control; comply with all applicable U.S. export regulations.

Other than that, the earliest possible return for positive ΔV is after four years, in 2053, with the 5:4 and 3:4 resonances (periods 0.8 yr and 1.33 yr, respectively).

A systematic search over the ΔV range of ±10 mm/s with 0.1 μm/s resolution reveals that resonant returns to impact within 25 years account for a few parts in 10,000 of the ΔV range. Almost half of this keyhole density is associated with the 7:5 resonance near -8 mm/s, which is not of concern for our ΔV > 0 scenario. Many more theoretically possible low order resonances do not appear in the Table 4 because they do not appear to support an impact. This is likely due to the presence of intervening approaches to Venus, Earth or the Moon that disrupt the resonant return (see Table 1). Moreover, later returns to impact tend to be eliminated through so-called MOID-sweeping, in which the asteroid's node precesses to the point that an impact is not possible, regardless of the arrival time. Some of the keyholes have been detected for tertiary impact years; these cases pass through a keyhole in a secondary b-plane. Near the selected 6:5 resonance, the numerical search for keyholes was reduced in step size from 0.1 μm/s to 0.01 μm/s to increase confidence that no significant keyholes were being missed. The locations of the major keyholes in Table 4 are depicted on the target plane in Figure 6 along with the corresponding circles predicted by Öpik-Valsecchi theory (Valsecchi et al. 2003). In this idealized model, the keyholes are located at the intersections of the resonant return circles with the line of variations. The actual miss distances in 2049 as a function of ΔV are depicted in Figure 7.

May contain Caltech/JPL proprietary information and be subject to export control; comply with all applicable U.S. export regulations.

Table 4. List of keyholes through 2074 in the 2049 target plane of 2016 NM4 as a function of primary deflection ΔV in the range +/-10 mm/s.

ΔV (mm/s)	Impact Year	Width (km)	Resonance
-8.0391	2062	0.2	Tertiary from 2054
-8.0217	2057	0.7	Tertiary from 2054
-8.0097	2054	49	7:5
-8.0050	2056	0.5	Tertiary from 2054
-7.9976	2065	0.07	Tertiary from 2054
-7.9905	2070	0.14	Tertiary from 2054
-4.6571	2065	10.3	23:16
-3.4484	2062	7.5	19:13
-1.2559	2070	1.1	31:21
-1.2314	2068	1.0	28:19
-1.2025	2066	1.5	25:17
-1.1649	2064	0.9	22:15
-1.1223	2073	0.09	Tertiary from 2062
-1.1073	2073	0.5	35:24
-1.0817	2060	1.0	16:11
-1.0202	2074	0.03	Tertiary from 2058
-0.9884	2065	0.4	23:16
-0.9020	2061	0.4	17:12
-0.8836	2066	0.1	24:17
-0.8732	2071	0.2	31:22
-0.7542	2068	0.1	26:19
-0.7261	2063	0.06	19:14
-0.6724	2052	0.3	4:3
-0.6427	2071	0.05	29:22
-0.6307	2065	0.04	21:16
-0.6207	2062	0.06	17:13
0.6403	2073	0.06	17:24
0.6688	2056	0.1	5:7
0.6955	2074	0.07	18:25
0.7051	2067	0.06	13:18
0.7267	2060	0.09	8:11
0.7664	2068	0.06	14:19
0.7764	2072	0.02	17:23
0.8165	2053	0.3	3:4
0.8608	2070	0.02	16:21

May contain Caltech/JPL proprietary information and be subject to export control; comply with all applicable U.S. export regulations.

ΔV (mm/s)	Impact Year	Width (km)	Resonance
0.8711	2066	0.06	13:17
0.8877	2062	0.07	10:13
0.9187	2058	0.2	7:9
0.9476	2063	0.09	11:14
0.9986	2054	0.3	4:5
1.0644	2060	0.2	9:11
1.1201	2055	0.3	5:6
1.1685	2062	0.04	11:13
1.2101	2056	0.3	6:7
1.2804	2057	0.3	7:8
1.3001	2074	0.1	22:25
1.3375	2058	0.2	8:9
1.3847	2059	0.2	9:10
1.4029	2070	0.03	19:21
1.6165	2069	0.05	19:20
1.6302	2070	0.1	20:21
1.8981	2050	2.4	1:1
2.2556	2069	0.2	21:20
2.3030	2067	0.3	19:18
2.3314	2066	0.2	18:17
2.5600	2061	0.3	13:12
2.6416	2060	0.6	12:11
2.6439	2070	0.02	Tertiary from 2060
2.8798	2058	0.6	10:9
4.3017	2065	1.5	19:16
4.3058	2070	0.07	Tertiary from 2065
4.4001	2070	0.9	25:21
4.6887	2054	5.5	6:5
4.6916	2058	0.01	Tertiary from 2054
4.6955	2063	0.03	Tertiary from 2054
5.0677	2073	0.07	Tertiary from 2068
5.9940	2071	0.11	Tertiary from 2062
6.0033	2067	0.02	Tertiary from 2062
6.0074	2062	5.3	16:13
6.0147	2066	1.1	Tertiary from 2062
7.2471	2066	0.08	Tertiary from 2053
8.9226	2068	0.18	Tertiary from 2064
8.9367	2064	10.7	19:15

May contain Caltech/JPL proprietary information and be subject to export control; comply with all applicable U.S. export regulations.

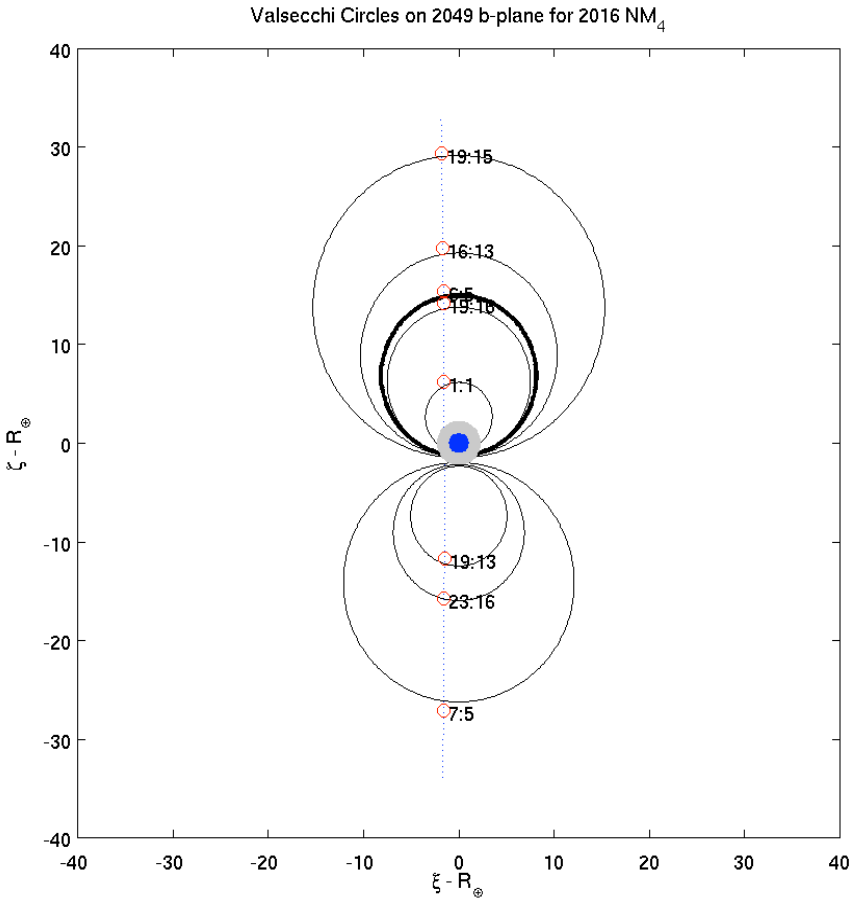

Figure 6. Selected resonant returns from the 2049 encounter on the 2049 target plane. The dotted vertical line marks the line of variations, i.e., the locus for kinetic ΔV in the range ±10 mm/s. The large black circles mark the loci for resonant returns under the idealized Öpik-Valsecchi model (Valsecchi et al. 2003). The red symbols mark the actual intersections of the resonant return and line of variation under the complete dynamical model. The blue dot marks the extent of the Earth, while the gray region marks the impact cross-section.

Gravity Tractor Phase

Although the probability of a kinetic deflection directly into a keyhole is only around 10^{-4}, the likelihood that the post-deflection uncertainty would intersect a keyhole is significantly larger. In the scenario contrived for this study, the gravity tractor would indeed be necessary to pull the asteroid away from the 6:5 resonance keyhole, and thereby avoid a secondary impact in 2054. There would be a relatively close approach to the Earth in Sept. 2046, at about 1 lunar distance that amplifies the 2049 b-plane deflection by a factor of 100 relative to that obtained on the 2046

May contain Caltech/JPL proprietary information and be subject to export control; comply with all applicable U.S. export regulations.

b-plane. This is not a particularly unusual scenario, but it would allow the gravity tractor to be more effective than it would be in the absence of close encounters.

The analysis of this effort takes place entirely in the 2049 b-plane, where the objective is simply to avoid the keyhole, rather than in the 2054 b-plane, where the analysis is more numerically challenging. In our simulation, the t-GT is capable of generating an acceleration of 2.5×10^{-12} m/s^2 or about 6.5 μm/s /month, and given the mass of the asteroid, the corresponding force is about 7.2 mN.

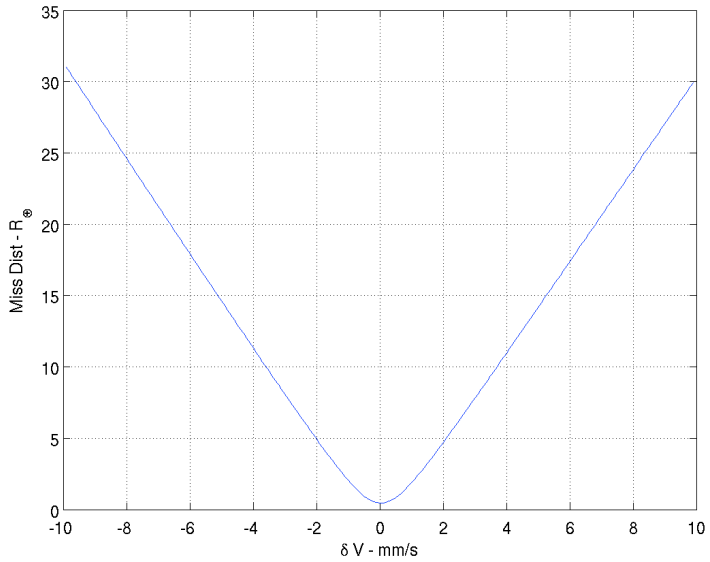

Figure 7. The miss distance in Earth radii on Sept. 12, 2049 vs. the tangential deflection in mm/s on July 4, 2028.

We allow at least a year after the mid-2028 IDM collision to re-establish the asteroid's orbit, determine that passage through the 6:5 keyhole is a significant possibility, and then make the decision to start tractoring well before the September 2049 keyhole passage. However, this would push the tractoring schedule into a period of time where deflections of any sort have a very low effectiveness, and this would force a delay in the tractoring for a few years. In this particular case, a three-year time interval centered on mid-April 2030 is inefficient to the point that it was avoided altogether. (See Figure 8.) This period of ineffectiveness is due to the presence of intervening close approaches between the deflection and the 2049 close approach. From Table 1, we note the asteroid makes a number of close approaches to Venus, Earth and the moon. Of particular interest for us is the relatively shallow 2036 encounter with Earth, at 0.034 AU. The geometry of this encounter is such that it tends to undo deflections that would be attempted in the months surrounding April 2030. Figure 8 shows how long the tractoring effort should last to effect a deflection of 750 km (three times the expected one-sigma uncertainty, as described in subtask 3). From that Figure we observe that the most efficient time to apply the low thrust deflection would be around 2037, when 750 km could be obtained in only about 50 days,

May contain Caltech/JPL proprietary information and be subject to export control; comply with all applicable U.S. export regulations.

although that same effect could be accomplished with less than 180 days of tractoring if the effort is initiated in 2032-2044. For the purposes of subtask 3, and before knowing what those results might be, we elect to start tractoring on July 4, 2032 for 200 days, which would yield a 2049 B-plane deflection of 650 km. (See Fig. 9.) As we shall see in the final analysis of Subtask 3, the 2049 b-plane one-sigma uncertainty is 260 km, so that the 650-km deflection is successful at the 650 km/260 km = 2.5 sigma level. An additional forty days beyond the simulated 200 days would bring the deflection to the 3 sigma level. Longer durations would provide ever-increasing statistical confidence in the miss. In practice, the start and length of the tractoring interval would be carefully selected to obtain the desired confidence in the primary objective of impact avoidance.

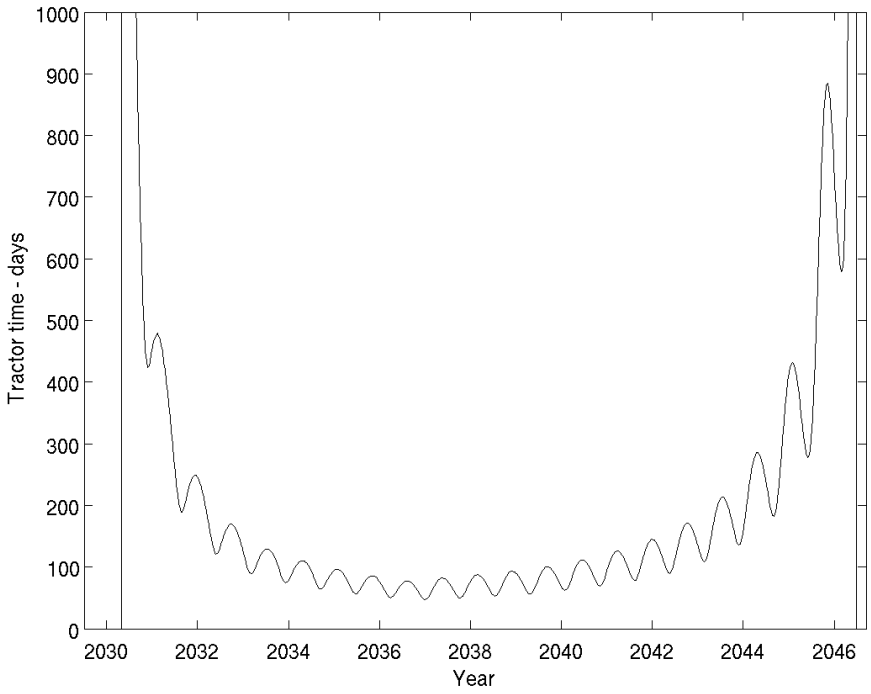

Figure 8. Tractoring efficiency as a function of start time. The plot shows the tractoring duration in days required to cause a deflection of 750 km on the 2049 b-plane. A shallow minimum exists from 2032 to 2043.

Inadvertently tractoring into an adjacent keyhole is obviously undesirable. However, the closest keyhole for a secondary encounter is over 6,000 km away in the 2049 b-plane, and this could only be reached after several years of tractoring. As shown by Table 4, our keyhole search has confirmed the existence of two nearby keyholes to tertiary impacts, and indeed there may be additional such keyholes below the resolution of our search. These keyholes are tiny – only tens of meters in width – and lie within 200 km of their associated primary keyhole. This second

May contain Caltech/JPL proprietary information and be subject to export control; comply with all applicable U.S. export regulations.

layer of nearby keyholes could be avoided by lengthening the tractoring time by another few months.

One might ask what the effectiveness of the gravity tractor would be if the 100:1 leverage afforded by the 2046 Earth encounter was not present. Under this alternate, hypothetical scenario, we assume that the size of the keyhole to be avoided is the same, only now it would be 6 km in 2046, rather than in 2049. The question is whether it would be practicable to steer the uncertainty footprint clear of the keyhole under this scenario, or equivalently, could the gravity tractor be effective in the absence of strong gravitational interactions. As we shall see later, from Subtask 3, the prediction uncertainty with a modest amount of post-tractoring tracking is about 3 km in the 2046 b-plane and 260 km in 2049 b-plane. Thus the gravity tractor would have to effect a deflection of up to the sum of 3 km (the semiwidth of the keyhole) and 9 km (to keep the 3-sigma ellipse clear of the keyhole. The absolute effectiveness of the gravity tractor in 2046 can be derived by reducing the computed 2049 deflection by a factor of 100. With this rescaling, Figure 9 reveals that the desired 12 km deflection in 2046 could be obtained with one year of tractoring starting on July 4, 2032, an amount not dramatically different from the duration required to clear the actual 2054 keyhole on the 2049 b-plane. The implication is that the strong dynamical effects of close planetary encounters (in the years between a deflection effort and the target plane) do not necessarily translate into correspondingly large reductions in the challenge of effecting a particular deflection. Rather, the leverage enlarges the uncertainty region at a rate comparable to the deflection effectiveness, and so the net effectiveness remains about the same.

Thus we have shown that the gravity tractor is a viable concept for providing a trim maneuver in our adopted strawman scenario. And, in all likelihood, it would be a viable concept for the majority of impact scenarios, although further study is needed to confirm this. Conversely, there might be possible scenarios with keyholes up to 2 orders of magnitude larger (or more), in which case the gravity tractor concept might not be adequate. Future threat possibilities would probably have to be analyzed individually and a customized deflection approach developed for each.

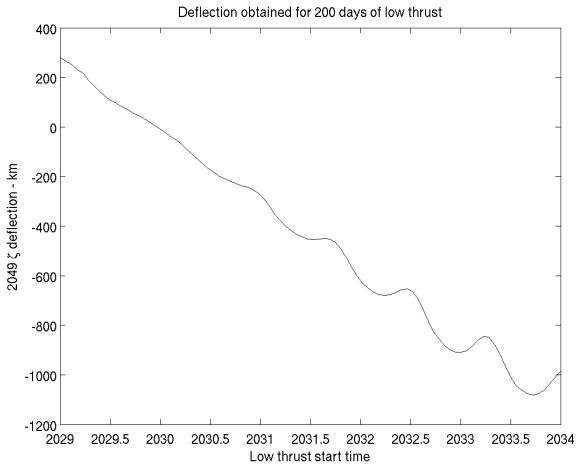

May contain Caltech/JPL proprietary information and be subject to export control; comply with all applicable U.S. export regulations.

Figure 9. Tractoring efficiency as a function of start time. The plot shows the size of the 2049 deflection along the line of variations after 200 days of tractoring for various tractoring start times.

Subtask 2: Study the gravity tractor spacecraft requirements to accelerate a NEO in a pre-determined direction and amount.

Subtask 2 Objectives

1. Choose a representative NEO model for all work that represents the median case (i.e., median of NEO size, aspect ratio, density, rotation rate, and orbit parameters as in above strawman target characteristics).
2. Demonstrate that a control law is possible that allows the spacecraft to hover in close proximity as the irregular NEO rotates beneath it.
3. Carry out a parametric analysis of station keeping performance in order to derive first-level requirements. Investigate the hovering and control distances to determine viability of station keeping. Run each case for 1 orbital period. Establish whether or not hovering and control are possible at close distances.
    a. Parameters (can be changed by joint agreement of JPL and B612 Foundation if results of initial analyses make it clear that parametric values are way off):
        1. S/C mass (500, 1000, 1500 kg)
        2. S/C range from NEO center of mass, keeping a to-be-determined margin of safety for NEO shape variations (parameters depend on NEO size and aspect ratio). Determine minimum acceptable stand-off distance for each case.
        3. Station-keeping box size and location
        4. Available thrust (use 5 engines and determine thrust levels required for each case; compare to available thrusters)
    b. Outputs: (for each case listed above)
        1. S/C accumulated delta-V/ thrust history required for maintenance
        2. Accumulated NEO movement as a function of time

1.4.3 Subtask 2 Results

1.4.3.1 Choose a representative NEO physical model

The representative NEO parameters we have selected for 2016 NM4 are largely covered as part of Subtask 1 in Table 2, including bulk density, rotation period, effective diameter, trajectory, and rotation pole.

The contribution to the definition of the representative NEO from this subtask is the shape and gravity model to be used. The shape chosen is the "rough model" of Itokawa defined by Ostro et al.(2005), scaled such that the volume of the shape is equivalent to the volume of a 70 m radius sphere (i.e., scaled to a 140 m effective diameter). Ostro et al.'s "rough model" of Itokawa *does*

May contain Caltech/JPL proprietary information and be subject to export control; comply with all applicable U.S. export regulations.

not include the shape information derived from the Hayabusa mission; it is however representative of those real data. The axial ratio of this model (1.95 x 1.08 x 1.00) is very close to the target value outlined in the proposal (2 x 1 x 1). Images of the shape model being used (with scale information) are shown in Figure 10.

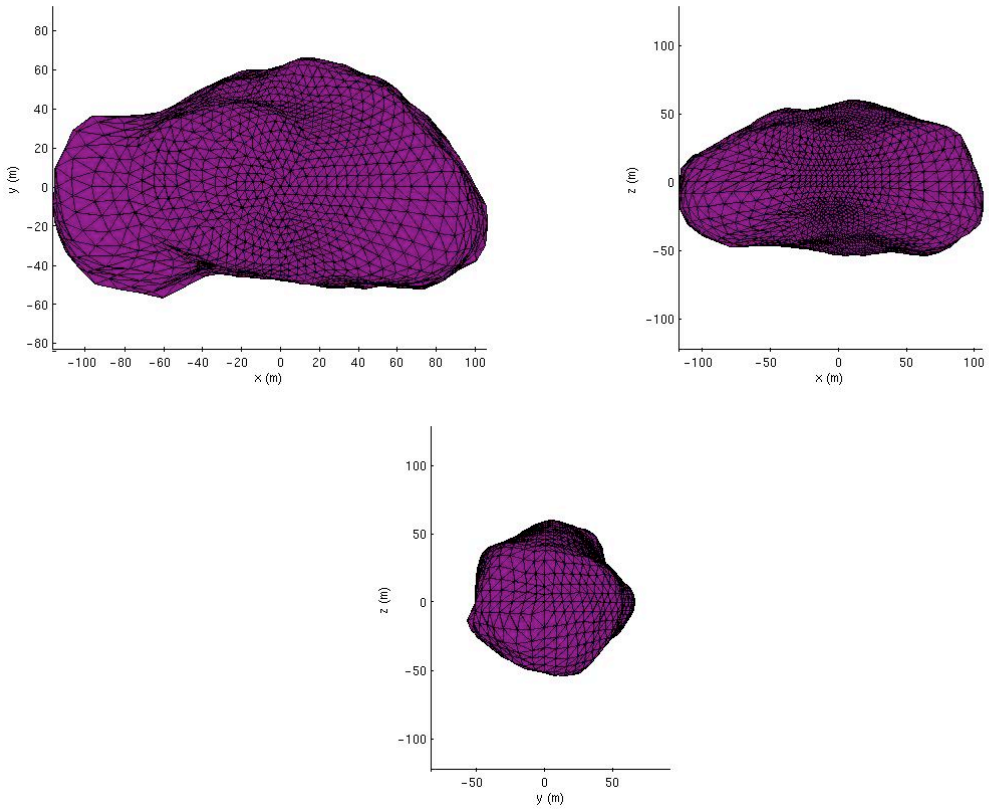

Figure 10. Images of the baseline asteroid shape. These are principal axis views where x is the axis corresponding to the minimum moment of inertia, y corresponds to the intermediate moment of inertia, and z corresponds to the maximum moment of inertia (i.e., the spin axis).

The gravitational potential model being used is defined by assuming the above defined shape has a uniform density value of 2.0 g/cm^3 (GM = 1.914 × 10^{-10} km^3/s^2) as described in Table 2. Accelerations derived from this model are computed using the method of Werner and Scheeres (1997).

1.4.3.2 Demonstrating that a control law is possible

May contain Caltech/JPL proprietary information and be subject to export control; comply with all applicable U.S. export regulations.

The second objective of Subtask 2 was to demonstrate that it would be possible to safely maintain sufficiently close proximity between a gravity tractor spacecraft and asteroid 2016 NM4 to exert the ΔV on the asteroid required to avoid impact in 2054 via a keyhole passage in 2049. To address this objective, we have created a high-fidelity software simulation of the translational spacecraft dynamics in the vicinity of our baseline model of 2016 NM4[3]. A thruster configuration and control law were developed to implement the stationary trajectory required for gravity tractoring to work. We have simulated the spacecraft dynamics under this thrust control for gravity tractoring durations of up to six months. The remainder of this subsection describes the spacecraft properties we have assumed, the simulation software, the thrust control law, and the results obtained in representative simulations of one and six month durations.

Preliminary Definitions:

The following coordinate frames are defined here to aid in understanding the discussion in this section.

"Asteroid Body-Fixed" coordinate frame

This non-inertial reference frame rotates with the asteroid such that the coordinates of any position on the asteroid surface are constant. The Z axis of this frame is aligned with the inertially-fixed rotation pole of the asteroid, which is parallel to the principal axis corresponding to the maximum moment of inertia of the 2016 NM4 shape model. The asteroid body-fixed coordinate frame rotates uniformly around its Z axis with respect to inertial space. The X axis of this frame is aligned with the principal axis of the asteroid shape corresponding to its minimum moment of inertia, i.e., the X axis is more-or-less aligned with the "longest" extent of the body. The Y axis completes the right-handed coordinate frame.

"Spacecraft" coordinate frame

This frame is defined to help us understand the orientation of the thrusters with respect to the desired gravity-tractor towing direction. The positive X axis of this frame points along the asteroid velocity vector; this is the desired towing direction. The positive Y axis is defined by the cross product of the X unit vector with the asteroid rotation pole direction. This vector points along the longitudinal direction with respect to the asteroid rotation pole. The positive Z axis is defined by the cross product of the X unit vector and the Y unit vector, completing the right-handed coordinate system. This vector points in the direction of changing latitude with respect to the asteroid rotation pole.

[3] Note that attitude dynamics were not simulated here. We have assumed that an attitude control system exists on the spacecraft that would be capable of maintaining the desired attitude for gravity tractoring. The desired attitude remains aligned with the velocity vector of the asteroid, so it changes quite slowly over time.

May contain Caltech/JPL proprietary information and be subject to export control; comply with all applicable U.S. export regulations.

Gravity Tractor Spacecraft Properties:

We have attempted to use realistic parameters in our simulation to model our gravity tractor spacecraft concept, though we haven't gone as far as doing a detailed spacecraft design. The following values were chosen for the spacecraft parameters with direct impact on the translational dynamics. The mass of the spacecraft at the beginning of the gravity tractor phase was chosen to be 1000 kg. The area of the spacecraft surface projected onto a plane perpendicular to the Sun direction was chosen to be 25 m^2. These values give a mass-to-area ratio of 40, which is an important parameter for computing the acceleration due to solar radiation pressure (SRP).

Given the power required to operate many solar electric propulsion (SEP) thrusters simultaneously, the 25 m^2 area would probably not be consistent with a spacecraft that is powered entirely by solar panels; we are in effect implicitly assuming a radioisotope thermoelectric generator (RTG) power or some other similar power source. If the mission were to be done with only solar power, there would be impacts on the spacecraft dynamics and control system, including increased demands on the attitude control system, decreased thrust accuracy (due to flexing of the solar panels), and some loss of tractoring ΔV efficiency due to larger SRP accelerations. These issues would increase the spacecraft development cost, but would probably not alter the feasibility of the mission.

Gravity Tractor Spacecraft Thruster Configuration:

We have assumed the gravity tractor spacecraft has 5 throttle-able fixed-direction SEP thrusters (not including backups) of which any three could be operated simultaneously. Each thruster is modeled after the ion thrusters used on the Dawn spacecraft, providing a maximum of 90 mN of thrust at a specific impulse (Isp) of 3100 seconds (Dawn spacecraft website, 2008).

The fixed orientation of the thrusters is defined with respect to the spacecraft coordinate frame (see "*Preliminary Definitions*" in this section) and is shown in Figure 11. Each thruster is represented by a red conical "nozzle" on the grey square spacecraft. Acceleration is applied to the spacecraft center of mass in the direction of the apex of the red nozzle when the thruster is fired. With this fixed thruster orientation, the spacecraft has the capability to apply control thrust in any direction in three-dimensional space.

The pair of thrusters labeled 'T1' and 'T2' apply force in the XZ plane of the spacecraft frame at an angle β away from the positive X direction. The angle β is the "thruster canting angle," which is further discussed in the part of this section on "*Selection of Tractoring Range.*" These thrusters generate most of the thrust required for the gravity tractor trajectory (since gravitational acceleration is primarily nulled by these thrusters) and act to control motion away from the nominal tractoring position in the negative X and +/-Z directions. The 'T3' thruster accelerates the spacecraft in the negative X direction. This thruster could be used as a safety net when the spacecraft gets much further from the body than the desired tractoring range and combines in a

May contain Caltech/JPL proprietary information and be subject to export control; comply with all applicable U.S. export regulations.

vector sense with 'T1' and 'T2' to create control thrusts that are purely along the Z direction. Finally, a pair of thrusters could be used to accelerate the spacecraft in the positive and negative Y directions, 'T4' and 'T5.' These thrusters would point roughly perpendicular to the average towing direction and are used for countering acceleration from solar radiation pressure, controlling unexpected perturbations in the Y direction, and countering the open-loop component of gravity that varies along the Y direction as the asteroid rotates.

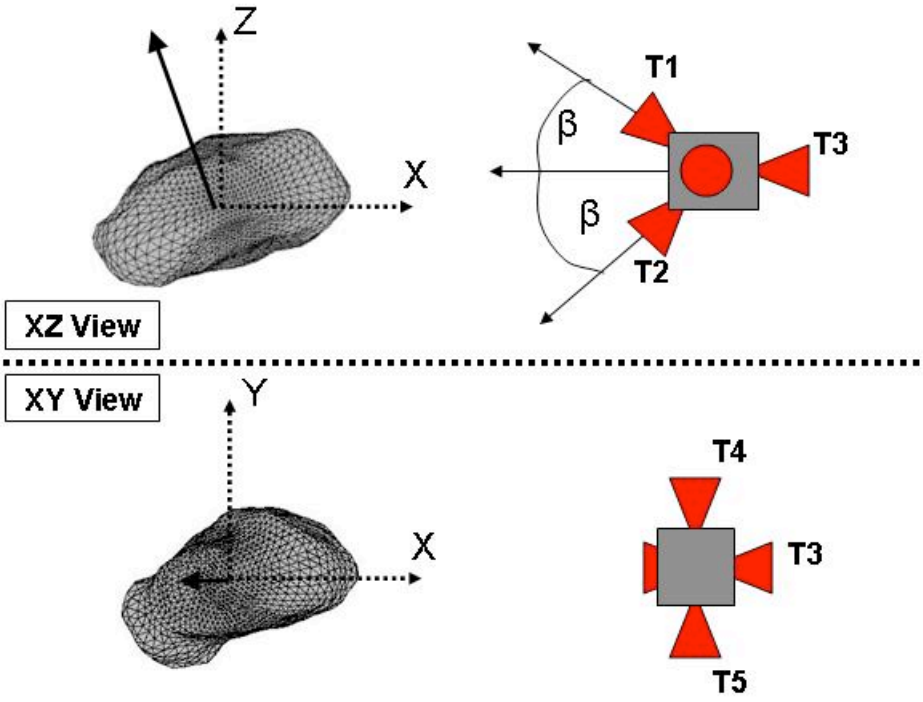

Figure 11: Diagram of the fixed thruster orientations on the gravity tractor spacecraft in the spacecraft coordinate frame. The heavy dark arrow originating at the asteroid represents its rotation pole.

Gravity Tractor Thrust Control Law:

In order to change the orbit of 2016 NM4, an acceleration must be applied to the asteroid that results in a secular change in its orbit elements. We have decided for this study that the most effective method of moving away from the 2049 keyhole is to change the asteroid orbit's semi-major axis. A quick examination of Gauss's equations governing the evolution of orbit elements under a low-thrust acceleration tells us the best way to change semi-major axis in a secular way is to apply acceleration along the asteroid's direction of motion (or in the opposing direction). Based on the workings of the gravity tractor concept (Lu and Love, 2005), the most efficient

May contain Caltech/JPL proprietary information and be subject to export control; comply with all applicable U.S. export regulations.

approach to changing the asteroid's semi-major axis is then to maintain a fixed spacecraft position along the asteroid's velocity vector[4].

We have selected a relatively simple dead-band control law to demonstrate the feasibility of tractoring for an extended period of time near 2016 NM4. The "dead-band" control approach allows us to define a bounding box around the (essentially) fixed tractoring position that we desire to which the spacecraft motion would restricted by thruster firings. This control concept has been successfully demonstrated in flight by JAXA's Hayabusa mission (Kominato et al., 2006). This type of control would be a good choice because it is robust against the fairly large amount of uncertainty in key environmental parameters (such as asteroid density and gravitational harmonics) that a mission could expect to have upon arrival at an asteroid.

The total spacecraft thrust applied under our control law is the vector sum of the contributions from two independent controller components. The first component is an open-loop thrust which acts to null the expected acceleration on the spacecraft at the nominal tractoring position. This component of thrust varies in both direction and magnitude with time as the asteroid rotates beneath the spacecraft and as the asteroid moves around the Sun.

The second component is the dead-band controller. This controller would confine the spacecraft motion to the region inside a specified dead-band "box" around the nominal tractoring position. The principal axes of the box are aligned with the basis vectors of the spacecraft coordinate frame (see discussion earlier in this section called "*Preliminary Definitions*"). When the spacecraft position is inside the box, no thrust is applied (from the dead-band component of the controller). When the spacecraft position is outside of the box along any of the spacecraft frame axes, thrust is applied along the dimension of the box that has been violated in the opposite direction of the violation as to accelerate the spacecraft back towards the box. If more than one dimension of the box is exceeded simultaneously, thrust is applied along all the dimensions that are violated.

The position dead-band controller described above has no damping and in the presence of uncertainty and finite duty cycles, spacecraft velocity could increase over time and eventually override the authority of the controller (Broschart and Scheeres, 2007). To stop this from happening, we place a restriction on the dead-band control law based on spacecraft velocity. As the spacecraft is accelerated back towards the dead-band box (when the dead-band thrust is active), the dead-band thrust would turn off when the spacecraft returns to the box or a maximum allowable speed in that direction is exceeded. This approach is effective at keeping the spacecraft velocity bounded over long tractoring durations.

[4] Technically, this exact position is generally not the optimal tractoring position when the asteroid has a non-spherical gravity distribution. However, for the purpose of argument and demonstration, it is close enough.

May contain Caltech/JPL proprietary information and be subject to export control; comply with all applicable U.S. export regulations.

Selection of Tractoring Range:

One of the most important decisions that must be made when designing a gravity tractor mission is at what range from the asteroid center of mass the spacecraft should be placed during the tractoring phase. Because the acceleration applied to the asteroid increases as the inverse square of the range, it is desirable to remain as close as possible in order to minimize the required tractoring duration to deflect the asteroid. Of course, the spacecraft must not be positioned so close that impact with the surface is a risk.

The maximum extent of our model for 2016 NM4 is ~117.3 m from the center of mass. This maximum occurs at roughly -4.2 deg latitude in the asteroid body-fixed coordinate frame (see frame definition above in the "*Preliminary Definitions*" part of this section). Though the spacecraft could be positioned inside of this distance for high-latitude tractoring positions, this distance would serve as a minimum threshold for all tractoring at all latitudes in the results reported here.

Another factor in determining the tractoring range might be avoidance of resonant excitation phenomenon. The synchronous orbit radius for our baseline asteroid is 131 m. It has been demonstrated that lateral (i.e., non-radial) motion of a spacecraft hovering (i.e., keeping the spacecraft position at a fixed position as we propose for tractoring) near this distance can be excited by this resonance (Broschart and Scheeres, 2005). Figure 12 shows the magnitude of the largest eigenvalue of the monodromy matrix corresponding to lateral motion after one rotation of the asteroid as a function of radial hovering range and latitude. In this plot, values greater than unity indicate instability in the lateral directions of motion, which in this case corresponds to resonant excitation. This is the case for tractoring locations in the triangular region on the left half of the plot. A gravity tractor spacecraft positioned at a location in the regions where there is no resonant excitation (right of the triangular region) should exhibit stable lateral motion. Tractoring in regions with the resonant excitation requires station-keeping control in all directions. Care must be taken to avoid excitation that could cause the spacecraft velocity to increase to the point it overwhelms the authority of the station-keeping control. There is some loss of ΔV efficiency when tractoring in the resonant area, but we will show in the simulation results later in this section that highly efficient use of ΔV would not be required to deflect 2016 NM4 away from the 2049 resonant-return keyhole. So we may conclude that this phenomenon is not a driver on the tractoring range unless the spacecraft is restricted to apply thrust along a single axis only, which would never be the case for this type of mission.

The final factor to consider when selecting a tractoring distance is the thruster canting angle required to avoid thruster plume impingement on the asteroid surface. The thruster canting angle β is defined as half of the angle between the two thrusters used to null gravitational acceleration on the spacecraft that point towards the asteroid (see the schematic representation in Figure 11; the canting angle is measured between 'T1' and 'T2'). The thrusters must be canted away from the asteroid direction so that the momentum of the particles coming out of the thruster would not be transferred to the asteroid surface; the resulting acceleration on the asteroid would work against the efforts of the gravity tractor. It is desirable for the thruster canting angle to be as

May contain Caltech/JPL proprietary information and be subject to export control; comply with all applicable U.S. export regulations.

small as possible to minimize cosine losses incurred when both thrusters are firing simultaneously (which would usually be the case).

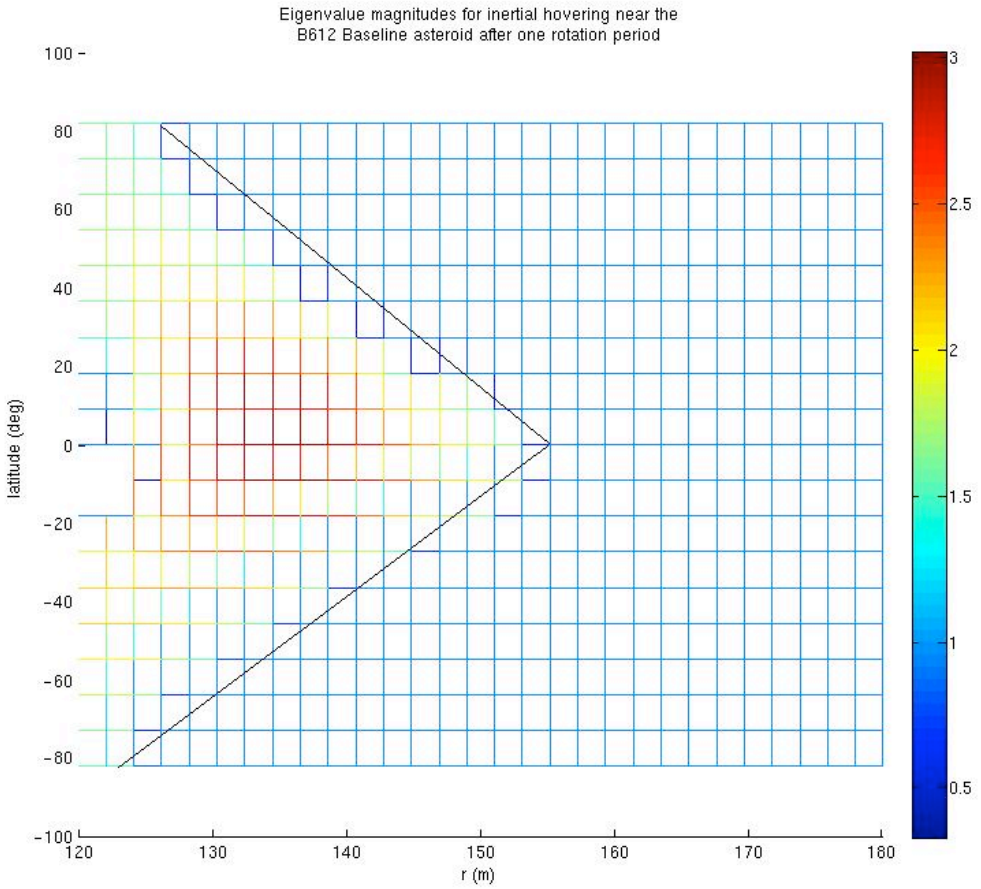

Figure 12: The magnitude of the largest eigenvalue of the lateral motion of a hovering spacecraft after one rotation period of the small body. Colors other than blue indicate resonant excitation.

To determine the minimum allowable thruster canting angle as a function of tractoring position, an oblate tri-axial ellipsoid (129.705 m x 129.705 m x 63.741 m) was first defined that circumscribes the baseline 2016 NM4 shape. This circumscribing shape must be an ellipsoid of rotation (oblate) because of the asteroid's rotation relative to the tractoring position. For the purpose of this analysis, the required thruster canting angle is computed as half of the angle between opposing vectors with base at the spacecraft that are tangent to the oblate ellipsoid surface plus a 5 deg margin. In general, the smallest possible minimum canting angle for a particular tractoring position will correspond to a thruster pair oriented in the XZ plane of the

May contain Caltech/JPL proprietary information and be subject to export control; comply with all applicable U.S. export regulations.

spacecraft frame. The largest possible minimum canting angle at a fixed tractoring position will correspond to a thruster pair oriented in the XY plane in the spacecraft frame. This is because the smallest dimension of the circumscribing ellipsoid lies in the XZ plane of the spacecraft frame. Figures 13 and 14 show the smallest and largest minimum canting angles allowable (respectively) as a function of tractoring latitude with respect to the asteroid equator and distance from the center of mass. Note that the canting angle required for thrusters in the XZ plane of the spacecraft frame is always smaller than the requirement in the XY plane. Larger canting angles correspond to reduced towing efficiency, so the thrusters should be canted in the XZ plane to maximize efficiency.

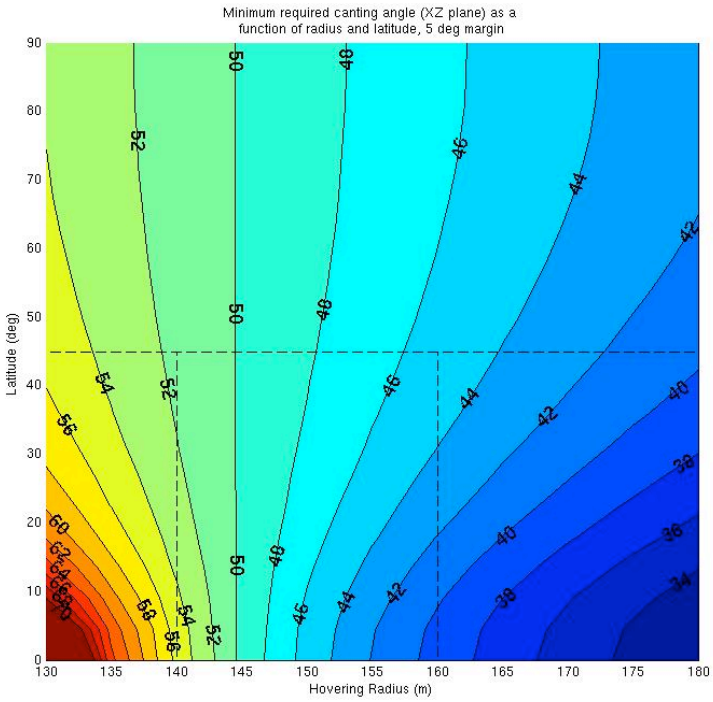

Figure 13: Minimum allowable thruster canting angle (degrees) for a thruster pair in the XZ plane of the spacecraft frame as a function of radial range from the asteroid center of mass and latitude with respect to the asteroid equator. This thruster orientation minimizes the required canting angle.

May contain Caltech/JPL proprietary information and be subject to export control; comply with all applicable U.S. export regulations.

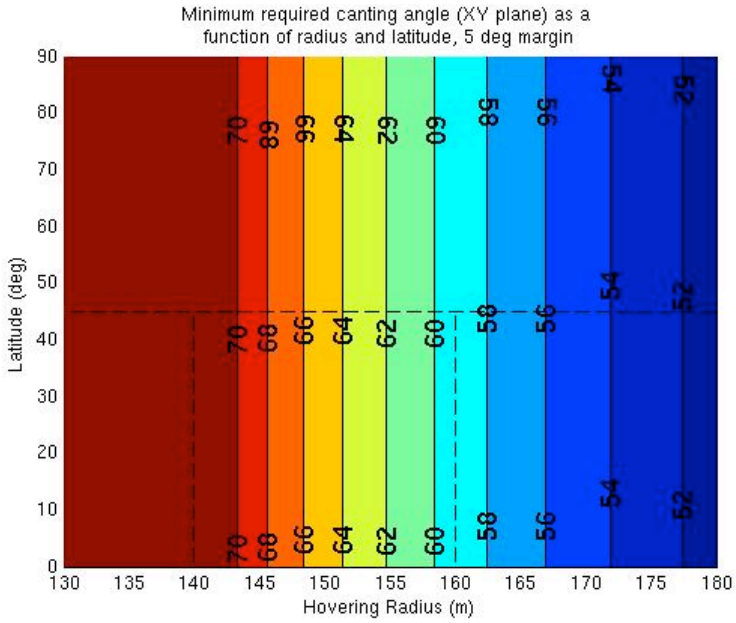

Figure 14: Minimum allowable thruster canting angle (degrees) for a thruster pair in the XY plane of the spacecraft frame as a function of radial range from the asteroid center of mass and latitude with respect to the asteroid equator. This thruster orientation results in the largest possible minimum canting angle for tractoring at a given location. (Values computed using a minor approximation. The value given is an upper bound on the true minimum.)

Gravity Tractor Trajectory Simulation Software and Inputs:

We have integrated the translational dynamics of the gravity tractor spacecraft under the control law specified above in the "*Gravity Tractor Thrust Control Law*" discussion using software written in Matlab©. The spacecraft attitude dynamics were not considered in this study. It was assumed that the attitude controller could maintain spacecraft alignment with the spacecraft coordinate frame without impacting the translational dynamics in any serious way.

The gravity tractor spacecraft dynamics were integrated using Matlab's 'ode45' integrator with the spacecraft equations of motion defined in an inertial reference frame. Forces on the spacecraft arising from the constant-density polyhedron gravity model (see section 1.4.3.1 and Table 2), solar radiation pressure (based on the model from Scheeres and Marzari, 2002), solar gravity, and the spacecraft's thrusters were included. The asteroid's position was specified by the ephemeris generated by Chesley and Chodas (2008). The asteroid's path was not modified by the spacecraft in the course of the simulation, but the forces induced on the asteroid by the spacecraft were recorded. The small motion of the asteroid relative to its original ephemeris

May contain Caltech/JPL proprietary information and be subject to export control; comply with all applicable U.S. export regulations.

would be a second-order effect in this simulation that would not be expected to have any significant bearing on the performance of the gravity tractor.

For these simulations, we have defined the desired tractoring position to be 155 meters from the asteroid center-of-mass along the asteroid's velocity vector. This will produce a tug on the asteroid that is roughly along the velocity vector, which will increase the semi-major axis of the asteroid's orbit around the Sun. The nominal 155 meters was chosen based on the criteria in the "*Selecting Tractoring Range*" discussion above as a reasonable compromise between towing force, spacecraft safety, and thruster efficiency (i.e., canting angle).

The size of the dead-band box boundary was +/- 25 meters from the desired tractoring position in the Y and Z directions (in the spacecraft frame). In the X direction, the "bottom" of the box is defined as 10 meters below the desired position and the "top" was 60 meters above the desired position. As an intermediate stage, if the spacecraft exceeded 10 meters above the desired position, all thrust in the X direction (including the open-loop component) was turned off. This was done for purposes of efficiency; the asteroid's gravity can be used to accelerate the spacecraft in the –X direction, saving fuel. The high limit of +60 meters in the X direction serves as a safety net, which has never been activated in any of the simulations we have run using the controller discussed here. The threshold velocity at which the dead-band thrust is turned off was selected to be 5 mm/sec in the X direction and 8 mm/sec in the Y and Z directions.

We have included uncertainties in the navigation solutions for position and velocity in the simulations. These navigation uncertainties were included in the simulation by the following methodology. At a fixed time interval, the on-board navigation solution was updated. This consisted of a random draw from a normal distribution for each component of position and velocity around the integrated trajectory solution. Each update of the filter was uncorrelated to the previous solution. The erroneous solution was then propagated forward as the "on-board estimate" along with the true solution. All thrust calculations made using the thrust control law were based on the on-board estimate. There were no differences between the dynamics used to propagate the on-board estimate and the true spacecraft state.

In the simulation data shown here, we assumed a 1-sigma uncertainty in each component of position of 1 meter and a 1-sigma uncertainty in each component of velocity of 1 mm/sec. These uncertainties are consistent with the performance expected from a spacecraft navigation system that incorporates altimetry, optical navigation, and radiometric measurements. Estimates of the spacecraft state were updated every 15 minutes.

May contain Caltech/JPL proprietary information and be subject to export control; comply with all applicable U.S. export regulations.

Table 5: Summary of Gravity Tractor Simulation Parameters for the Spacecraft and Thrust Controller

Spacecraft Initial Mass:	1000 kg
Spacecraft Area (normal to Sun-line, fixed value)	25 m^2
Number of Thrusters	5
Maximum Thrust (per thruster)	90 mN
Thruster Isp (constant)	3100 seconds
Thruster Canting Angle	50 degrees
Tractoring Range	155 meters
Position Dead-band Limit (X direction)	+/-10 meters, + 60 meters
Position Dead-band Limit (Y and Z direction)	+/-25 meters
Dead-band Thrust Cutoff (velocity threshold in X direction)	5 mm/sec
Dead-band Thrust Cutoff (velocity threshold in Y and Z directions)	8 mm/sec
Position Uncertainty (1 sigma in each component)	1 meter
Velocity Uncertainty (1 sigma in each component)	1 mm/sec
Navigation Filter Update Frequency	Every 15 minutes

Gravity Tractor Trajectory Simulation Results:

Using the setup described above, spacecraft trajectories subject to our control law were integrated for periods of 1 day, 5 days, 1 month (8 independent runs), and 6 months (2 independent runs). The relative tolerance used was $1x10^{-4}$ and the absolute tolerance was $1x10^{-6}$. In this document, we will show the results from a single one month period and a single six month period. Both periods begin on July 4, 2032. All of the runs we have done exhibit the same qualitative properties as the data shown here. Data from other runs can be obtained by request. In all cases, our control law was successful in keeping the position of the spacecraft near the desired tractoring position and exerting the expected level of acceleration on 2016 NM4.

Figure 15 shows the spacecraft trajectory (blue) for the 1-month and 6-month integrations relative to the 2016 NM4 center-of-mass in an inertial coordinate frame aligned with the asteroid fixed frame at the initial epoch. Note that in this frame, the desired tractoring position migrates around an inclined circle as the asteroid moves around the Sun (i.e., as the asteroid velocity vector rotates in inertial space). The spacecraft trajectory tracks this slow drift in the desired tractoring position well, as shown by the "smear" of the blue trajectory around roughly half a "tractor orbit" relative to the body. The "tractor orbit" is inclined due to the obliquity of the

May contain Caltech/JPL proprietary information and be subject to export control; comply with all applicable U.S. export regulations.

asteroid's pole with respect to its orbit around the Sun. Also note that the asteroid shape is rotating in this frame. The shaded area around the asteroid represents the circumscribing oblate ellipsoid filled by the asteroid as it rotates.

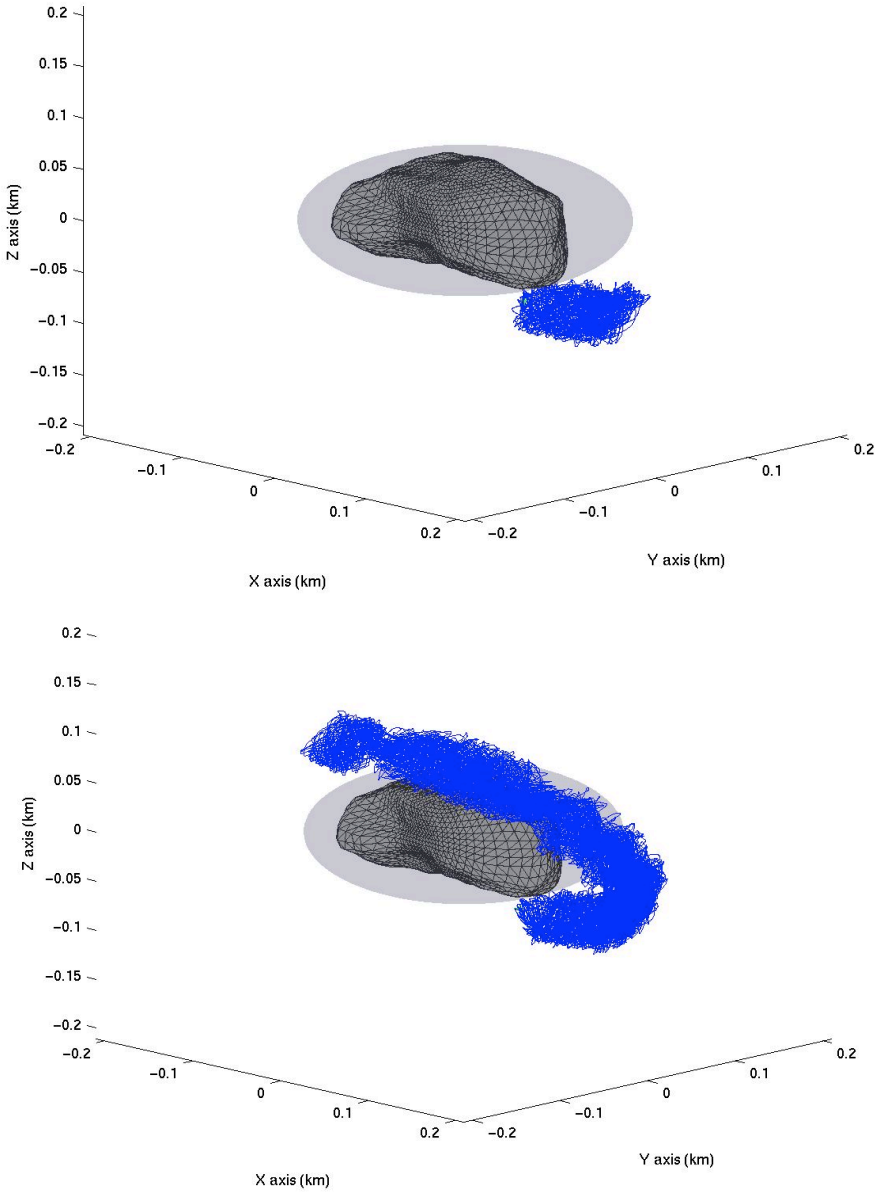

Figure 15: Spacecraft trajectory relative to 2016 NM4 (inertial coordinate frame). Top: 1 month integration, Bottom: 6 month integration.

May contain Caltech/JPL proprietary information and be subject to export control; comply with all applicable U.S. export regulations.

Figure 16 shows the same spacecraft trajectories as in Figure 15 in the asteroid body-fixed coordinate frame. Each time the asteroid rotates beneath the spacecraft in an inertial frame (every 6 hours), the trajectory would trace out an "orbit" in this frame. Over the course of the 2016 NM4 orbit around the Sun, the latitude of the desired tractoring position shifts with respect to the fixed asteroid equatorial plane (see Figure 15), which causes the latitude of these "orbits" to drift. Over the course of one-half of 2016 NM4's heliocentric orbit, the tractoring trajectory traces out a spherical surface segment from +45 deg latitude to -45 latitude in this frame (as shown in the 6 month result).

Figure 17 shows both spacecraft trajectories relative to the desired tractoring position. This figure may be most helpful is assessing the effectiveness of our control law at keeping the spacecraft near the desired tractoring position. In this figure, the blue line represents the actual spacecraft trajectory and the red dashed line shows the on-board estimate of position. Note how the on-board estimate makes sudden changes; this corresponds to times when the estimate is updated. It can be seen here that our controller does an excellent job of keeping the spacecraft in the desired region around the desired tractoring position. The negative X, negative Y, and positive Y boundaries of the position dead-band control are clearly visible (-10, -25, and + 25 meters respectively). Excursions beyond the dead-band boundary are minimal, which tells us that our station-keeping thrusters have sufficient thrust to do their job well. Remember that at the positive X boundary, thrust is only turned off instead of reversed, so the excursions outside the box are a little larger on that side. Also note that the "safety net" dead-band at +60 meters in the X direction is never needed. The perspective of these figures only shows the X and Y deviations, but the Z direction is similarly well bounded (as Figure 18 shows). Also, if you look closely at the 1 month figure, you can see that the trajectory "web" is denser around the area where the Y deviation is zero. This corresponds to motion early in the trajectory that is primarily up and down relative to the asteroid. Eventually perturbations set in and the motion becomes more irregular, filling the entire box (Evidence of this effect will also be seen in Figure 20, where the difference between the tractoring ΔV and the ΔV applied to the spacecraft is minimal near the beginning of the simulations).

Figure 18 shows each component of the spacecraft deviation from the desired tractoring position as a function of time. This is the same data as shown in Figure 17 plotted as a function of time. The red line represents the deviation along the spacecraft frame X coordinate, the blue line shows deviation along the Y coordinate, and the green line shows deviation along the Z coordinate. Again, you can see that the position dead-band boundaries in the X, Y, and Z directions are well respected by the spacecraft trajectory. Note that when the trajectory goes from the maximum to the minimum and back repeatedly in any particular coordinate, that means that the primary oscillation of the spacecraft around the desired tractoring point is in that direction at that time. For pretty much the entire duration, the trajectory bounced back and forth between the X boundaries; this is because the trajectory is unstable in that direction. At times, the spacecraft also traverses the entire width of the dead-band box in the Y or Z directions repeatedly as well.

May contain Caltech/JPL proprietary information and be subject to export control; comply with all applicable U.S. export regulations.

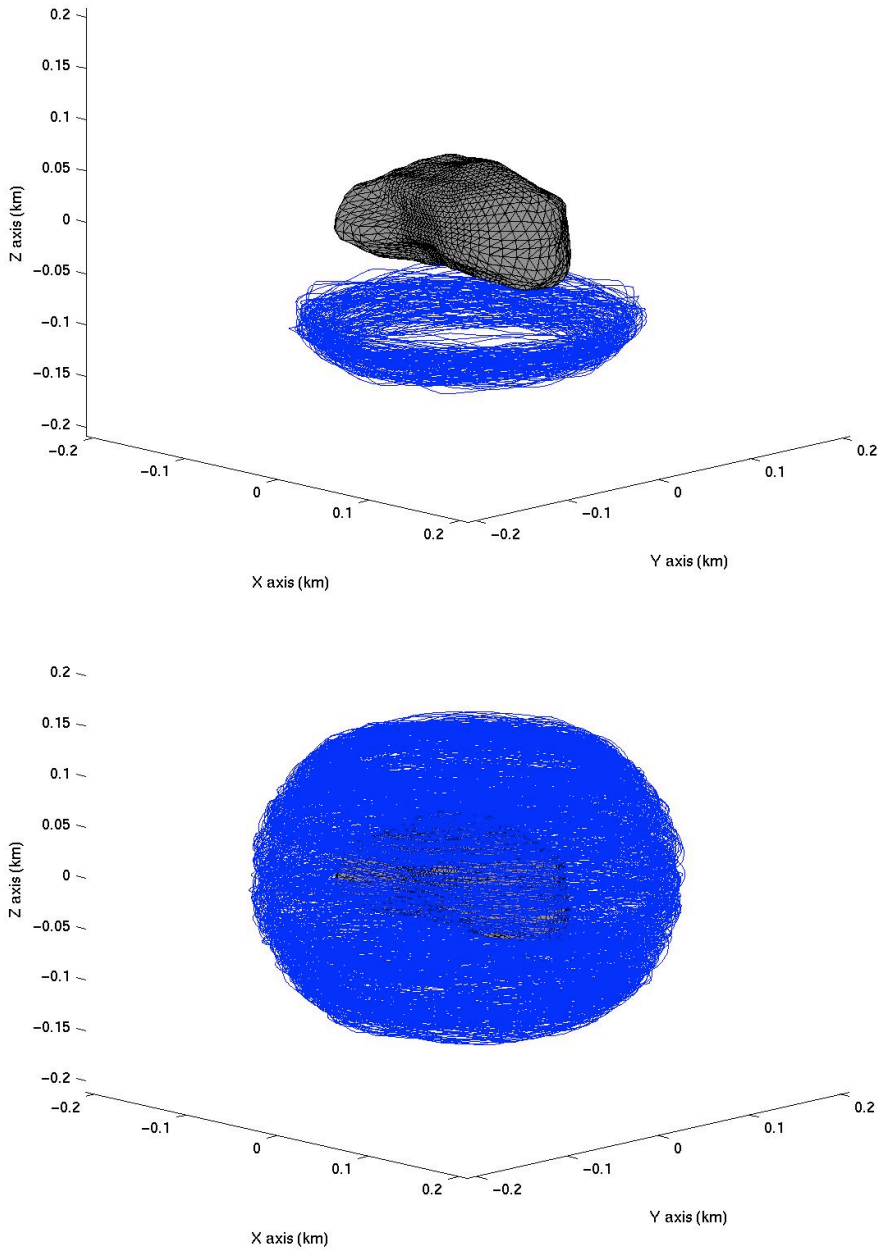

Figure 16: Spacecraft trajectory relative to 2016 NM4 (asteroid body-fixed coordinate frame). Top: 1 month integration, Bottom: 6 month integration.

May contain Caltech/JPL proprietary information and be subject to export control; comply with all applicable U.S. export regulations.

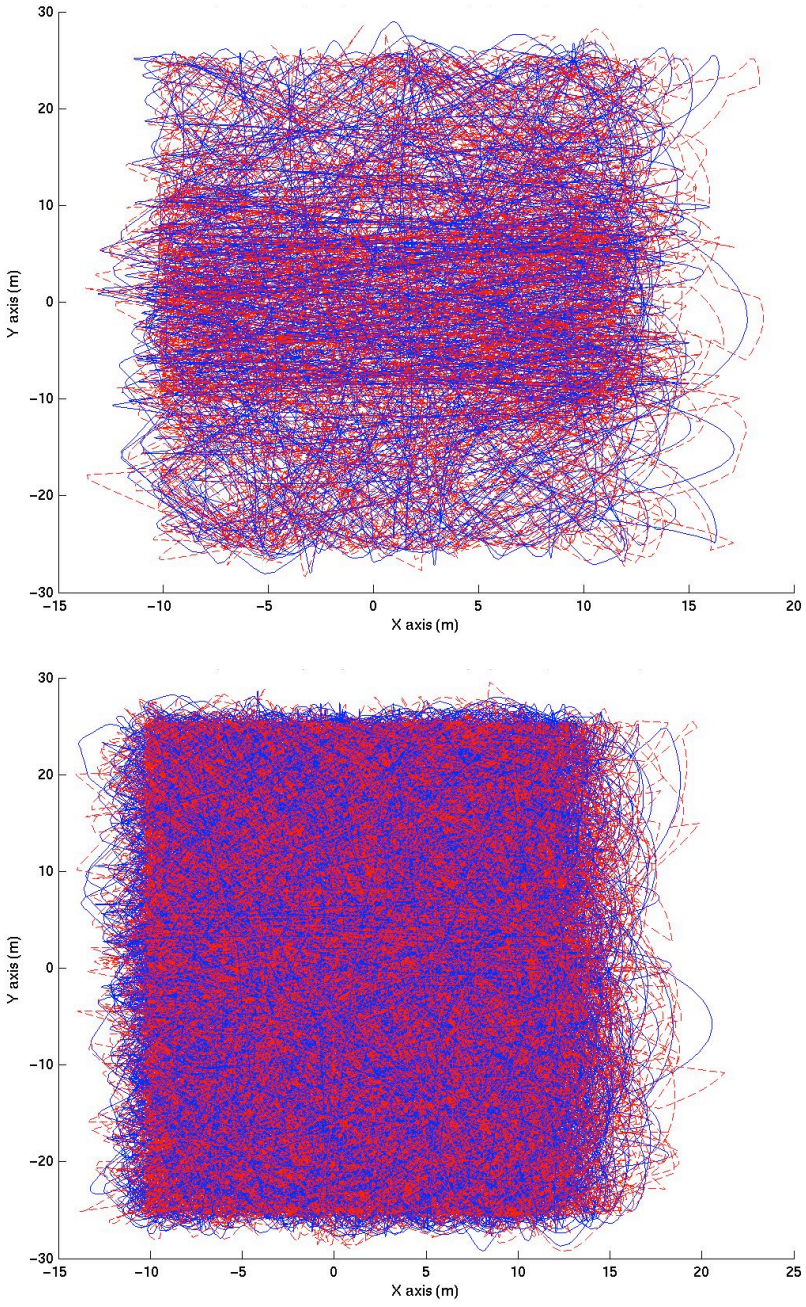

Figure 17: Spacecraft trajectory relative to the desired tractoring position (spacecraft coordinate frame). Top: 1 month integration, Bottom: 6 month integration.

May contain Caltech/JPL proprietary information and be subject to export control; comply with all applicable U.S. export regulations.

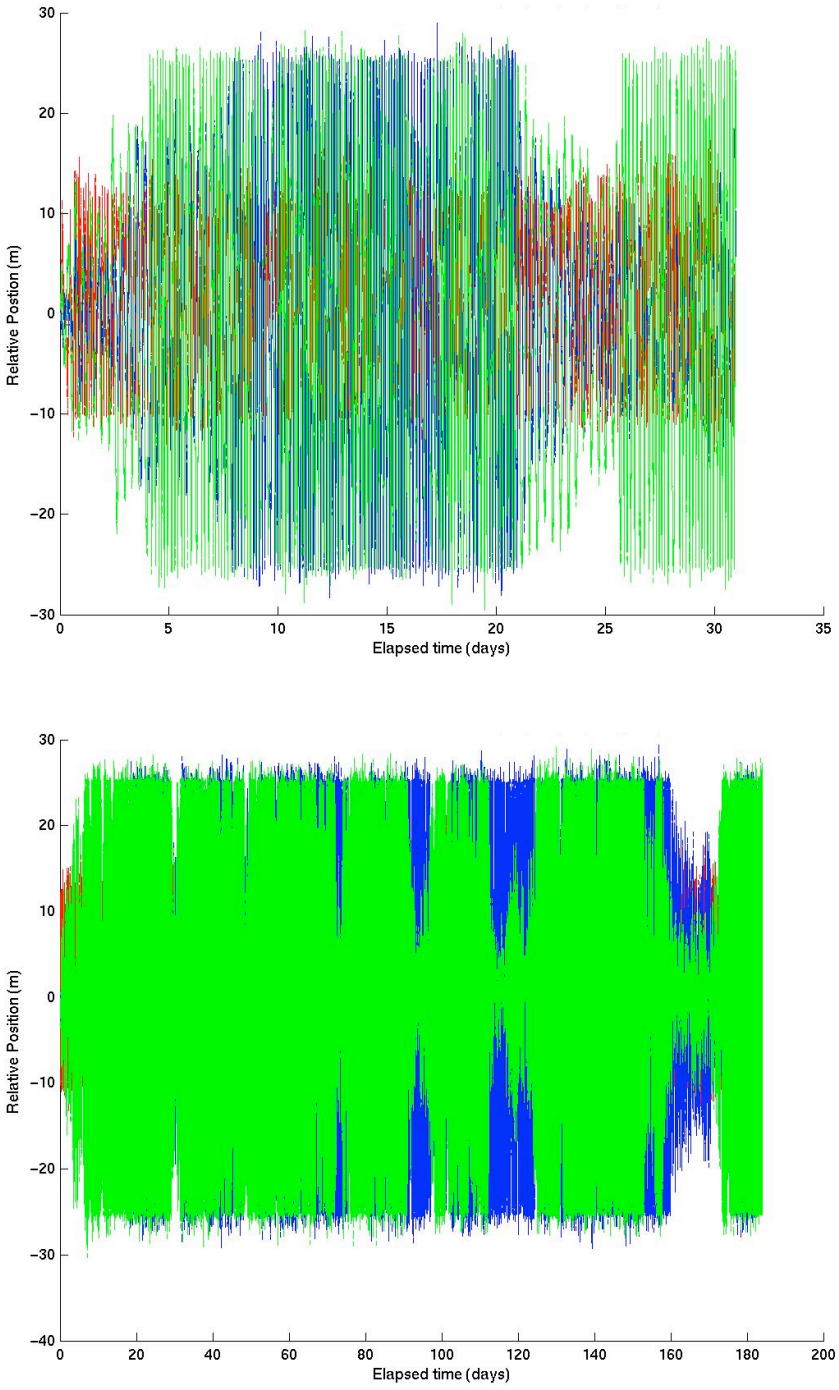

Figure 18: Components of spacecraft position relative to the desired tractoring position (spacecraft coordinate frame) as a function of time. Red: X coordinate, Blue: Y coordinate, Green: Z coordinate. Top: 1 month integration, Bottom: 6 month integration.

May contain Caltech/JPL proprietary information and be subject to export control; comply with all applicable U.S. export regulations.

Figure 19 shows each component of spacecraft velocity as a function of time. It can be seen that the spacecraft velocity remains well bounded over time and does not grow in a monotonic way. This is a good thing because if velocity was increasing over time, the dead-band control authority would eventually be overwhelmed and control of the spacecraft would be lost. This demonstrates that the return velocity threshold included in the dead-band portion of the control law is effective at damping any excess energy that arises from uncertainties. Recall though, that the limit on velocity is only imposed when the dead-band thrust is active along that particular axis. Therefore, the speed in any particular direction could be larger than the threshold when the position dead-band thrust is not active. This can be seen here on many occasions. The point of the velocity threshold is not to hold the spacecraft speed below some threshold, but to keep the kinetic energy of the spacecraft bounded.

Figure 20 shows the ΔV used by the simulated spacecraft thrusters as a function of time. The red line shows the total ΔV expended by the spacecraft, defined as the sum of the ΔV used by each thruster. The blue line shows the applied ΔV, defined as the integral over time of the total thrust vector magnitude. The green line shows the tractoring ΔV, defined as the ΔV required to counter the component of gravitational acceleration along the velocity vector of the asteroid. This quantity can be thought of as the ΔV used to move the asteroid along its velocity vector.

Efficiency measures can be defined from these quantities. Let the "thruster efficiency" be defined as the applied ΔV divided by the total ΔV expended. This number describes the loss due to applying thrust in a vector direction with a fixed thruster orientation. This loss is primarily driven by the thruster canting angle required to avoid having the thruster plume impinge on the asteroid surface. Let the gravity tractor efficiency be defined as the tractoring ΔV divided by the total expended ΔV. This tells us the fraction of the total expended ΔV that is being used to accelerate the asteroid along its velocity vector. This number includes losses due to thrust vectoring, station-keeping thrust, and oscillation of the pull direction due to the irregular shape of the body. Figure 20 shows that for the one month period shown, the simulated spacecraft expends a total of 40.91 m/s of ΔV; 63.2 percent of which is used to accelerate the spacecraft (thruster efficiency) and 48.4 percent of which is used to pull the asteroid (gravity tractor efficiency). For the 6 month case, 261.3 m/s of ΔV is expended with a thruster efficiency of 63.6 percent and a gravity tractor efficiency of 46.8 percent. Note that all ΔV costs grow at a consistent rate over time. Also, these efficiency numbers were consistent to within a few percentage points across the simulations performed.

May contain Caltech/JPL proprietary information and be subject to export control; comply with all applicable U.S. export regulations.

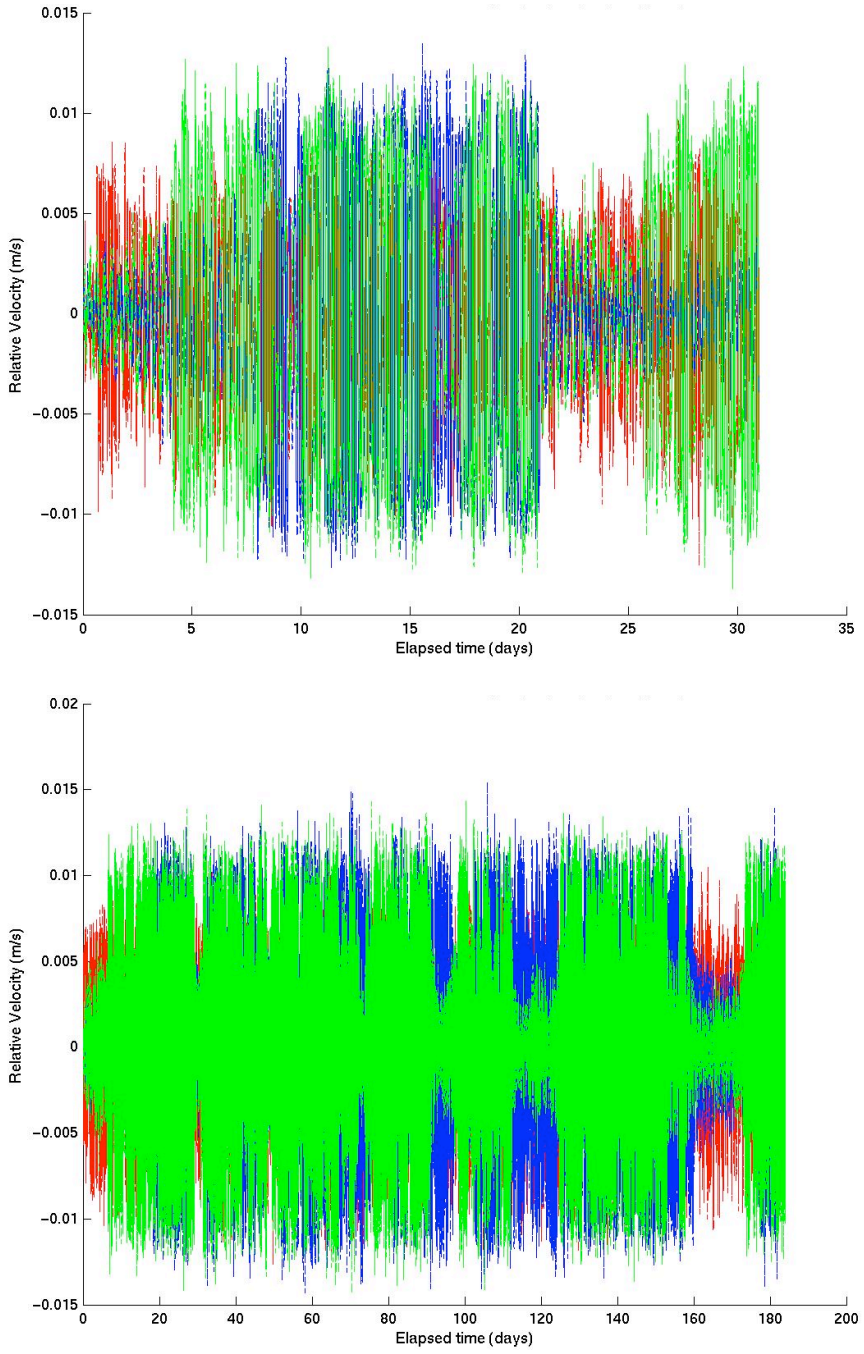

Figure 19: Components of spacecraft velocity (spacecraft coordinate frame) as a function of time. Red: X coordinate, Blue: Y coordinate, Green: Z coordinate. Top: 1 month integration, Bottom: 6 month integration.

May contain Caltech/JPL proprietary information and be subject to export control; comply with all applicable U.S. export regulations.

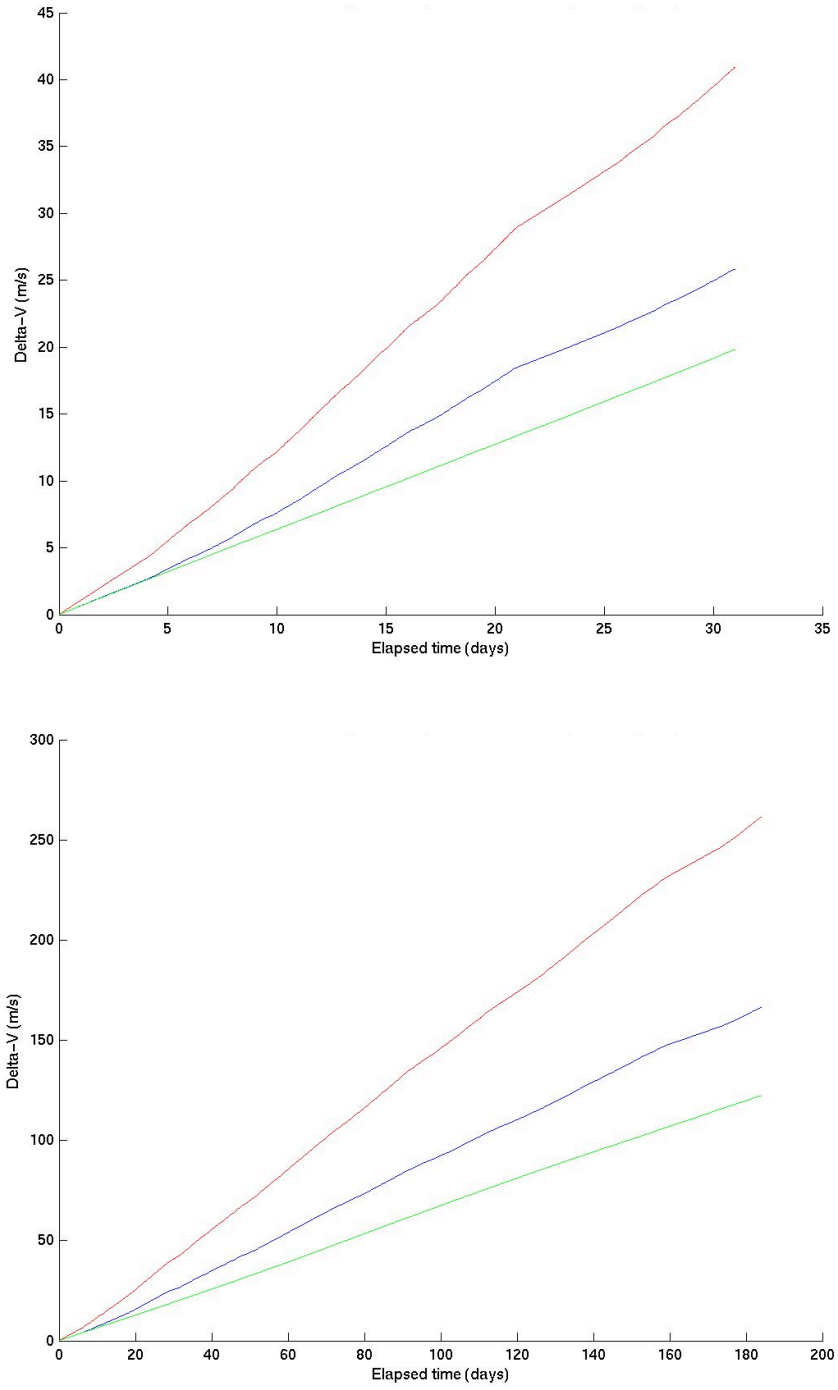

Figure 20: Spacecraft ΔV consumption versus time (Red is total ΔV consumed, blue is total ΔV applied to spacecraft, green is total ΔV used to accelerate the asteroid). Top: 1 month integration, Bottom: 6 month integration

May contain Caltech/JPL proprietary information and be subject to export control; comply with all applicable U.S. export regulations.

Figure 21 shows the spacecraft mass as a function of time. Because of the high Isp of the ion propulsion thrusters and the small accelerations experienced by the spacecraft at 2016 NM4, the rate of propellant mass consumption (for translational thrust) averages only about 1.4 kg per month of tractoring. Over the 6 month period beginning on July 4, 2032, the spacecraft consumes only 8.6 kg of propellant to perform gravity tractoring. Note that over the 6-month period, some small variations would be expected in the mass consumption rate due to variations in tractoring latitude with respect to the asteroid and variance in the use of the lateral station-keeping thrusters. This effect is present, but its magnitude is minimal.

Figure 22 shows the time variation in magnitude of the simulated spacecraft acceleration due to thrust. The vector magnitude is shown in red and the sum of the thrust magnitudes for each thruster is shown in blue. Each individual thruster is limited to a maximum thrust of 90 mN, as is the total thrust vector magnitude. However, when more than one dead-band boundary is violated simultaneously, the sum of the thrust magnitudes can be larger (blue line). Note that a thrust of 90 mN roughly corresponds to an acceleration of 0.9×10^{-4} m/s^2 for a 1000 kg spacecraft. The low level of thrust that would be active for the majority of the time corresponds to the open-loop control thrust component.

Figure 23 shows the total ΔV applied to the asteroid along its velocity vector as a function of time. This plot tells us how well the simulated gravity tractor is working. It can be seen here that the rate of increase in the total ΔV applied to 2016 NM4 is very consistent; the primary variations (which are not really visible) are due to the seasonal change in tractoring latitude with respect to the asteroid. This is because the ΔV on the asteroid is only a function of spacecraft positions (and the masses), which would vary very little when the tractoring controller is working well (see Figures 17 and 18). The small variations in position around the desired tractoring position have a negligible effect in this simulation. It can be seen from these simulation results that a total ΔV of about 7 μm/s is applied to the asteroid each month in the scenario we have simulated here. This means that our spacecraft can exert sufficient ΔV to divert 2016 NM4 from the hazardous 2049 keyhole in a matter of months under this control law (see Table 4).

Figure 24 shows the angular deviation of the simulated spacecraft from the asteroid velocity vector as a function of time. The goal of our controller was to maintain this angle close to zero, which was achieved. To get a truly optimal gravity tractoring control law, this would vary somewhat so that the gravitational acceleration vector acting on the spacecraft and asteroid was aligned with the asteroid velocity vector, which is not necessarily the same as what we've done because of the irregular shape of the asteroid. This would allow for small gains in efficiency, but as seen by the modest total propellant mass expended in Figure 19, the savings of a few grams of fuel are not that important. The key here is to keep this angle small so that the cosine loss of the actual gravitational acceleration is small.

May contain Caltech/JPL proprietary information and be subject to export control; comply with all applicable U.S. export regulations.

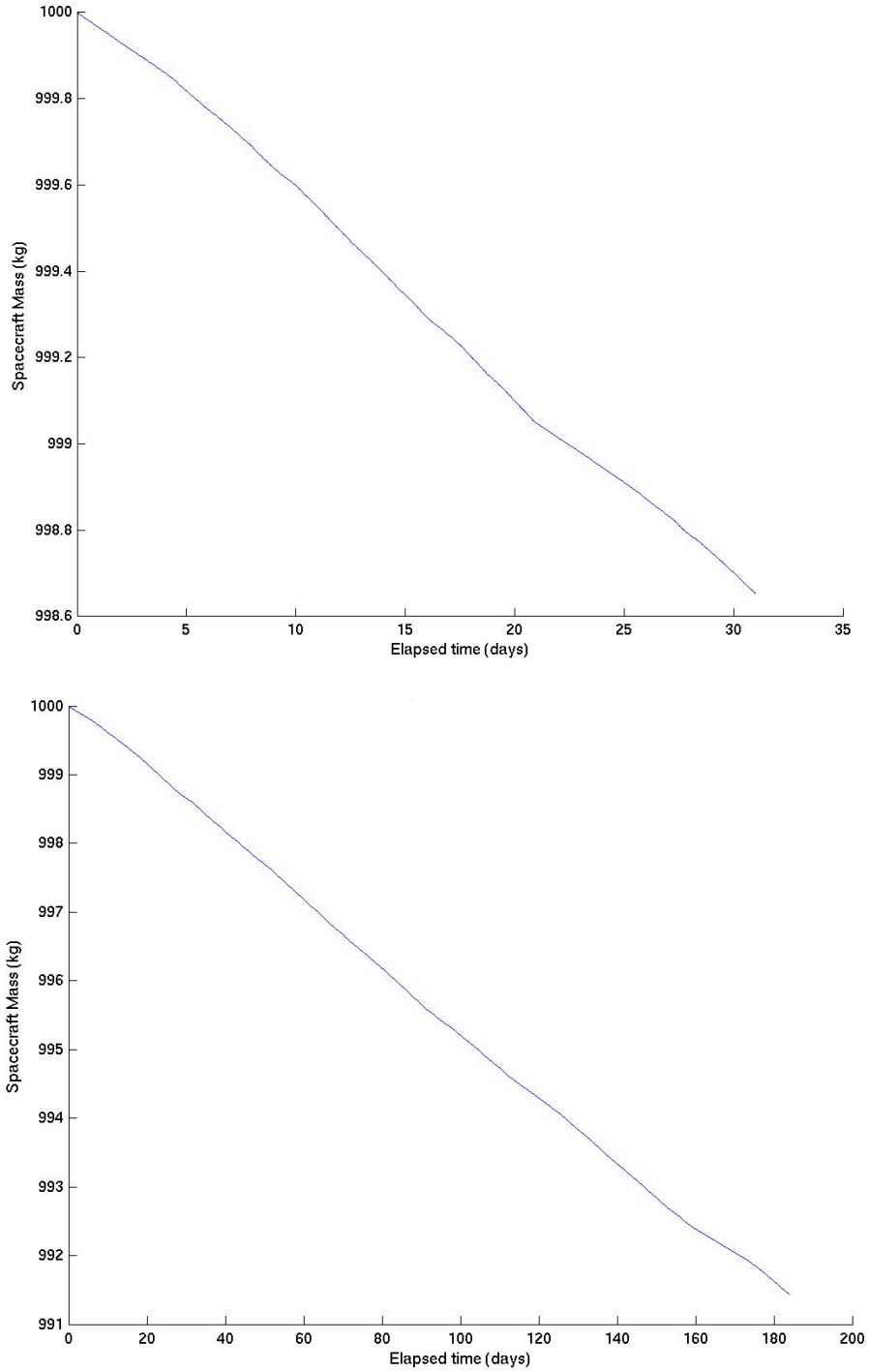

Figure 21: Simulated spacecraft mass versus time. Top: 1 month integration, Bottom: 6 month integration.

May contain Caltech/JPL proprietary information and be subject to export control; comply with all applicable U.S. export regulations.

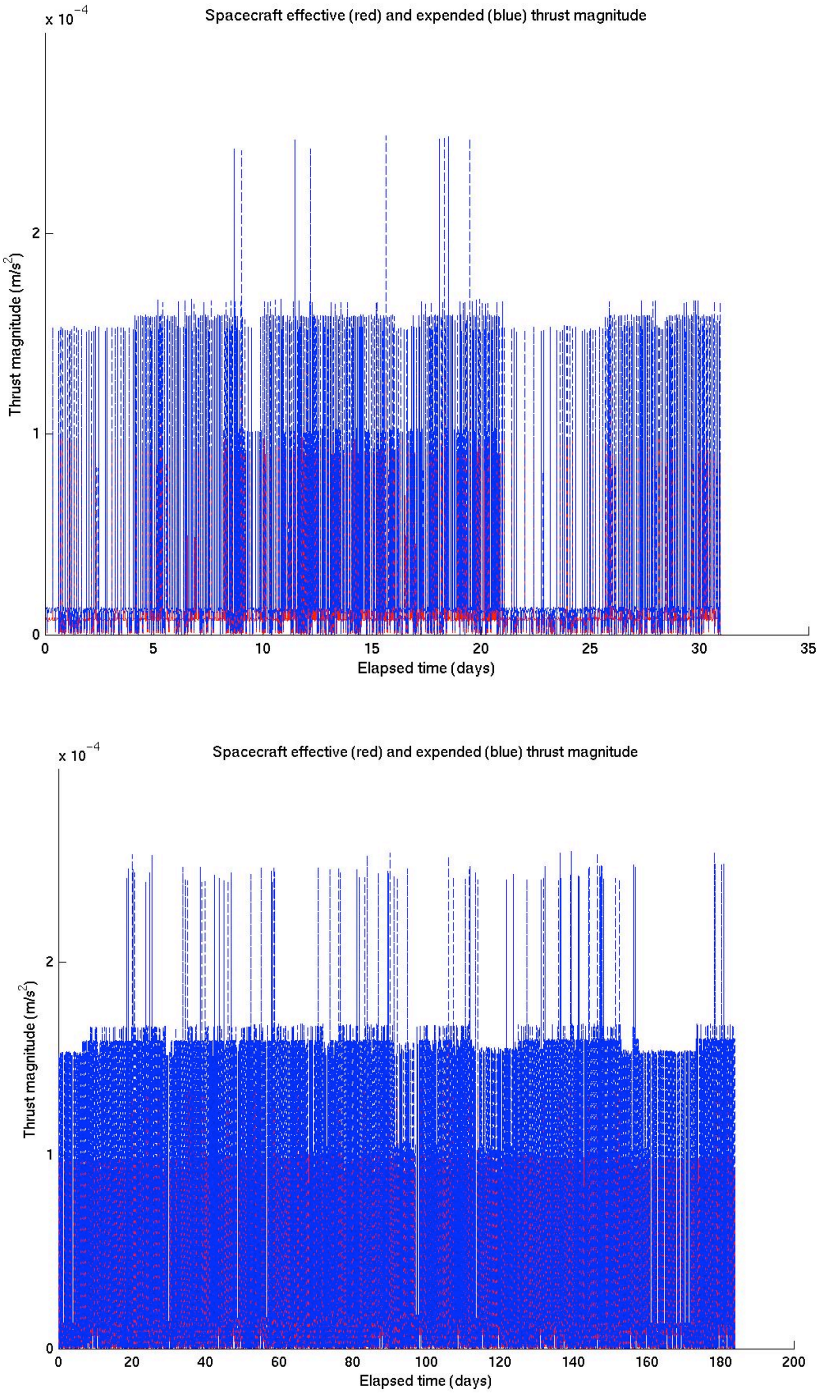

Figure 22: Spacecraft acceleration from thrust versus time.Top: 1 month integration, Bottom: 6 month integration.

May contain Caltech/JPL proprietary information and be subject to export control; comply with all applicable U.S. export regulations.

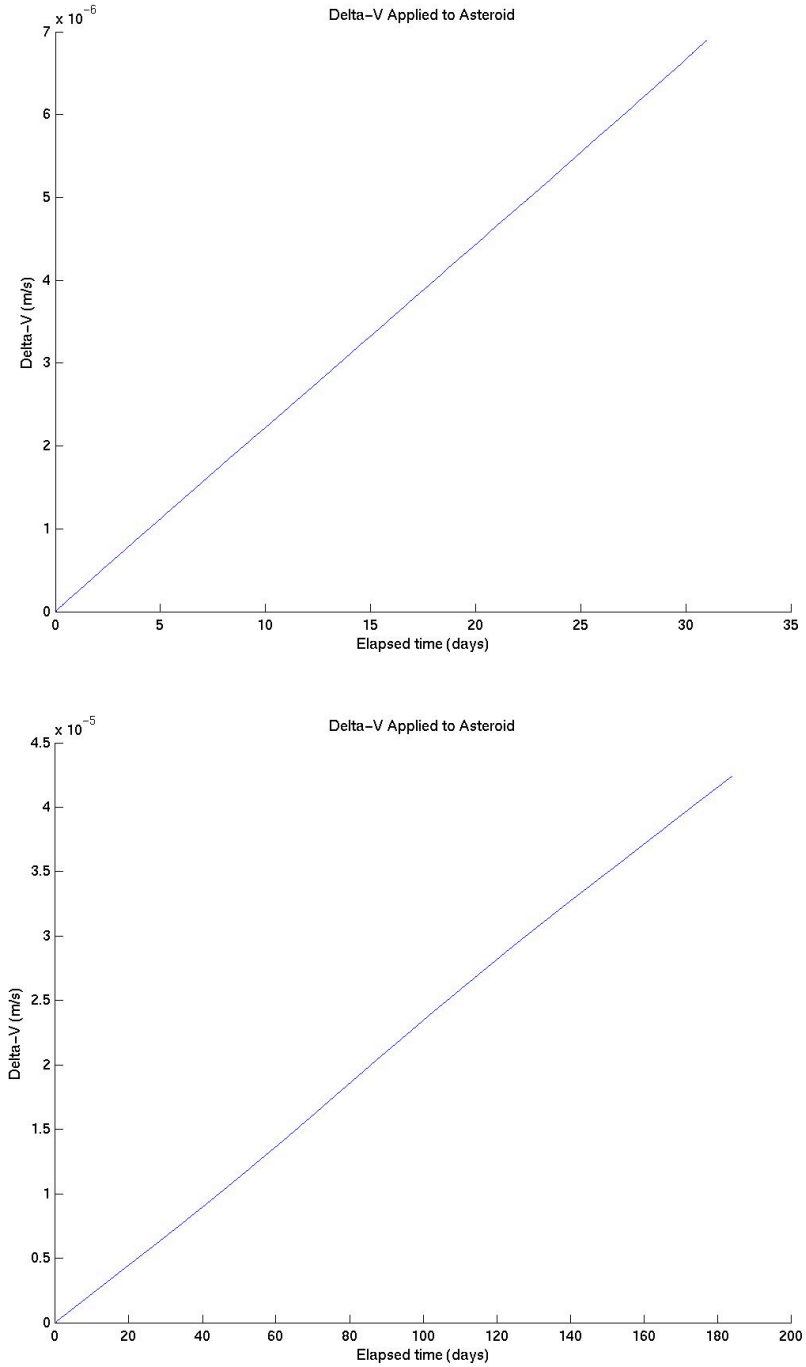

Figure 23: ΔV applied to 2016 NM4 along its velocity vector versus time. Top: 1 month integration, Bottom: 6 month integration.

May contain Caltech/JPL proprietary information and be subject to export control; comply with all applicable U.S. export regulations.

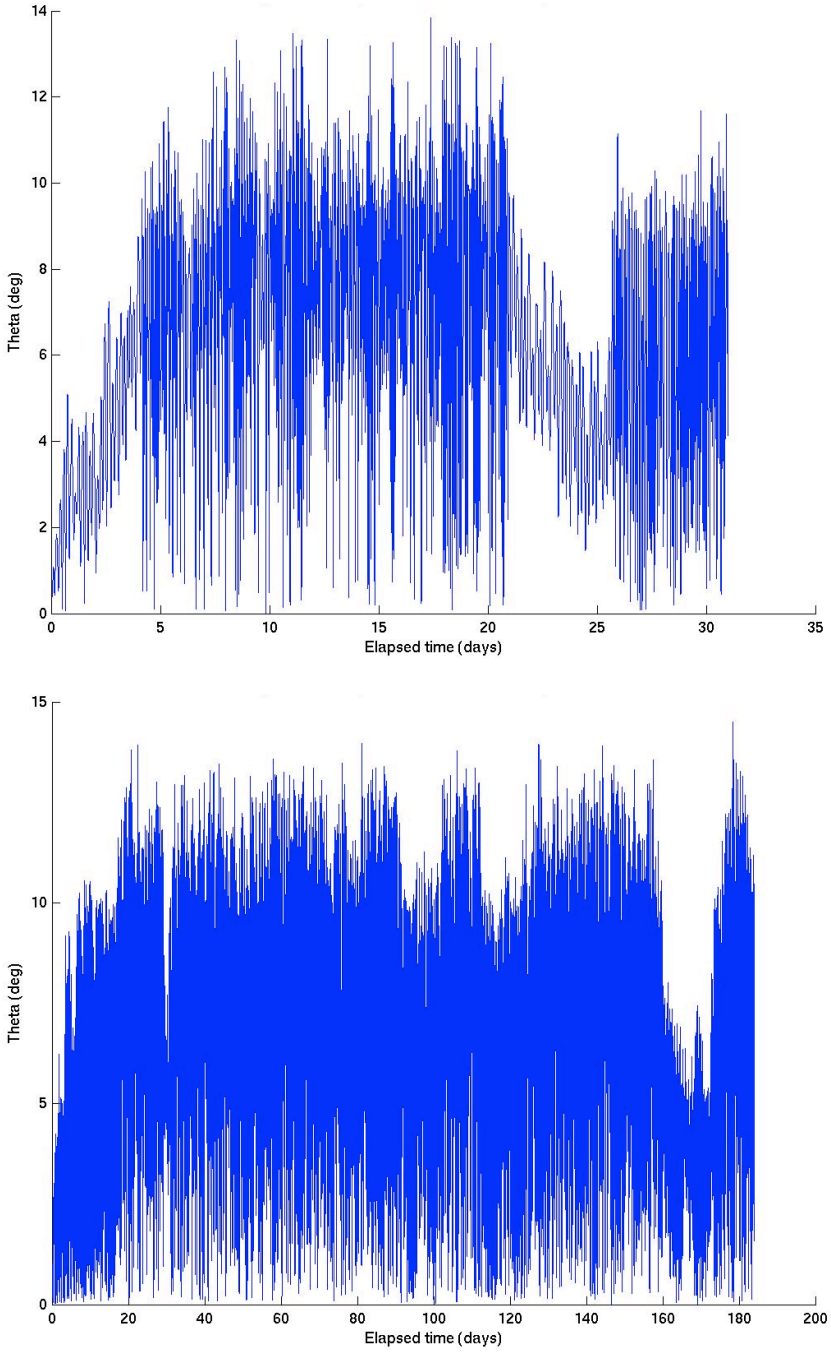

Figure 24: Angle between the spacecraft position and the asteroid velocity vector versus time. Top: 1 month integration, Bottom: 6 month integration.

May contain Caltech/JPL proprietary information and be subject to export control; comply with all applicable U.S. export regulations.

Summary and Discussion

Using a high-fidelity numerical simulation, we have demonstrated the use of a thrust control law that could safely maintain the spacecraft positioning required for the gravity tractor phase of our mission when there is navigation uncertainty in the spacecraft state. The same simulations have shown that tractoring for a matter of months near 2016 NM4 at a range of 155 meters from the center-of-mass is sufficient to safely accelerate the asteroid by the amount required to avoid a keyhole in 2049. An effort was made to make realistic assumptions about the spacecraft properties and capabilities throughout (though a detailed design was not done).

One item of particular interest was the very small amount of propellant mass required to do the job. This suggests that for a mission with similar requirements to our baseline mission, SEP propulsion might not be required; chemical options might be sufficient.

In future work, the robustness of our control could be further tested by utilizing an imperfect on-board dynamics model. This would create error in the open-loop portion of the thrust control law, which would probably decrease the ΔV efficiency, but not make the controller ineffective unless the error was very large (orders of magnitude larger than the nominal acceleration itself). Adding an imperfect dynamics model would also cause the on-board state estimate error to grow larger as it is propagated forward between updates. This would probably not break the control law either. Error in the thrust application could be added as well. If thruster application error (which could reflect attitude uncertainty as well) and dynamics uncertainty were included, in addition to navigation uncertainty, the tractoring control law could be put through a rigorous test of its robustness.

1.4.3.3 Carry out a parametric analysis of station keeping performance

In this section, some questions put forth in the proposal document are addressed. They are addressed here as discussion topics in light of the simulation results and experiences.

Viability of Tractoring at Close Proximity

A discussion of tractoring distances was given in the discussion entitled "*Selection of Tractoring Range*" in Section 1.4.3.2. The conclusions were that tractoring should occur at no less than the maximum radius of the circumscribing ellipsoid (~130 meters for 2016 NM4) from the center-of-mass. Some margin is required on that number depending on the size of allowable deviations from the nominal tractoring position, uncertainty in the asteroid shape, and dimensions of the spacecraft. Outside of this minimum radius, our simulations and analytical data suggest that any range is doable, though the higher required canting angles for low altitude tractoring positions decreases the ΔV efficiency. Figure 12 also suggests a more simplistic and more efficient controller might suffice beyond a range of about 160 meters. This notion however was not tested via simulation.

May contain Caltech/JPL proprietary information and be subject to export control; comply with all applicable U.S. export regulations.

Varying the Spacecraft Mass

These results are very nearly spacecraft mass independent. That is to say, they scale very cleanly with initial spacecraft mass within a reasonable range. The ΔV applied to the asteroid would be changed from the values given here as the ratio of the new mass divided by 1000 kg. The fuel consumed by the spacecraft would change in the same way (though the percentage of spacecraft mass consumed by the thrusters will be the same). Given the same thruster performance capabilities, the control law would become less effective as the spacecraft mass increases; it would allow deviations further and further outside of the box until it becomes a problem. The mass would probably have to increase by at least an order of magnitude before that happened. In that case, larger thrusters or banks of thrusters would remedy the situation.

Varying Range from the Center-of-Mass

All else equal, varying the target tractoring range from the center-of-mass would vary the towing force (and therefore, the applied ΔV) by roughly the inverse square of the ratio of the distances. Assuming the control law keeps the spacecraft near the desired position, the only parameter that affects the ΔV on the asteroid is the spacecraft position through the gravitational acceleration, which has roughly an inverse square scaling.

Regarding the spacecraft ΔV efficiency, there will be some improvement as the tractoring range is increased since the required canting angle would be reduced and a simpler control law with less station-keeping thrust might be possible.

Varying Station-Keeping Box Size

In the simulation data shown here, the station-keeping box was set to allow a maximum deviation of 10 or 25 meters depending on the direction. This is a fairly small value, but appropriate due to the close proximity to the surface and the danger of resonant phenomenon arising during long ballistic segments (for close tractoring). Because of our focus on tractoring so close to the body, it might not be practical to vary this parameter much as part of a parametric analysis. A smaller box would probably decrease the efficiency somewhat and could become a problem with respect to uncertainty in spacecraft state and dynamics.

Comments on the Required Thrust versus Available Thrusters

For the baseline scenario studied here, the limitations imposed by the Dawn ion thrusters had no adverse impact on controller performance. As mentioned above, if the spacecraft were much more massive, larger thrusters might be required.

May contain Caltech/JPL proprietary information and be subject to export control; comply with all applicable U.S. export regulations.

Subtask 3: NEO Tracking.

The key question to be addressed in this subtask is:

What is the time evolution of NEO ephemeris errors that would be obtained by a station-keeping spacecraft equipped with a standard X-band transponder in the immediate vicinity of a NEO? This question is to be understood in the context of the following scenario:

Suppose a NEO is on course to potentially impact the Earth at a future date (the impact epoch). Approximately 20 years before the impact epoch, a rendezvous t-GT spacecraft, equipped with altimetry, optical navigation, and radio transponder instruments, is maintaining station in the vicinity of the threatening NEO and verifies whether or not the potential impact would occur. If the potential impact is confirmed, we suppose that a deflection attempt is carried out. The t-GT spacecraft would then be used to verify that the deflection maneuver was sufficient to prevent the Earth impact, and furthermore to determine whether the NEO is headed for any keyholes in the impact plane that would lead to a subsequent Earth impact. If passage through a keyhole is a possibility, the t-GT spacecraft could be used to "tow" the NEO to move its trajectory away from the keyhole. The spacecraft would move in very close to the NEO to perturb it onto a non-threatening trajectory via the mutual gravitational attraction of the spacecraft and NEO. This GT mode would be maintained until the NEO was confirmed to be on a safe trajectory.

Specific questions to be addressed through this subtask are:

1. Considering that the *a priori* uncertainty in the effectiveness of the deflection technique is very large (i.e., the momentum multiplier, β, is poorly known), how soon after the deflection epoch could the primary deflection be confirmed?
2. When would the uncertainties on the target plane at the 2049 impact epoch be comparable to the scale of the secondary impact keyholes that are to be avoided? Similarly, if the NEO is indeed deflected onto a secondary impact trajectory, how soon would this be recognized as likely?
3. Assuming that a secondary impact is found to be very possible, and the rendezvous spacecraft is then employed as a gravity tractor, how quickly could the GT deflection be measured? Could the deflection be adequately inferred through the thruster history? Could it be explicitly measured more or less in real time?

The nature of the NEO trajectory and in particular its close encounter history during the years from the deflection epoch to the impact epoch is crucial in determining the uncertainty at the impact epoch. This task attempts to examine this issue by subdividing the analysis into two parts: first, the NEO ephemeris uncertainty at the time of the observations, and second, the uncertainty mapped to the impact epoch.

May contain Caltech/JPL proprietary information and be subject to export control; comply with all applicable U.S. export regulations.

Overview

The purpose of this subtask is to quantify the ability to precisely determine the orbit of the asteroid by tracking a spacecraft in orbit or hovering near the asteroid using standard radiometric and optical navigation techniques. The scenario assumed for this study is as follows. First, an orbiter spacecraft would arrive at the asteroid in early January 2028, about 6 months prior to the arrival of an impactor spacecraft. During this 6 month period, the orbiter would be tracked from the Earth to obtain a very precise orbit of the asteroid prior to impact. Next, the orbiter would be maneuvered to a safe position and the impactor would hit the asteroid on July 4, 2028, imparting a change in velocity ΔV to the asteroid. Soon thereafter, the orbiter would be maneuvered back to the asteroid and then tracked in order to measure the ΔV that was imparted. After a period of time in which a high accuracy measurement of the ΔV is obtained, the gravity tractoring portion of the mission begins. Following the tractoring phase, the orbiter would once again be tracked to determine the net acceleration imparted to the asteroid. The three primary questions to be addressed in this subtask are:

1. How accurately could the pre-impact orbit of the asteroid be determined? This accuracy could be parameterized by the amount of time prior to impact that the spacecraft is tracked, as well as the combinations and accuracies of the data types.
2. How many days/weeks/months of spacecraft tracking following the impact would it take to determine the impact ΔV to a sufficient accuracy?
3. How many days/weeks/months of spacecraft tracking following the gravity tractoring phase does it take to determine the acceleration imparted by the tractor to a sufficient accuracy?

In all cases, "sufficient" accuracy is defined as the level needed to ascertain whether or not the asteroid is on an Earth impacting trajectory. In principle, the most obvious way to determine the orbit of the asteroid *in situ* would be to land a transponder on the surface and track the radio signal of this beacon from the Earth. This method, however, has some operational problems that might be difficult to overcome, including power and thermal issues for a landed spacecraft encountering extended and recurring periods of darkness due to the asteroid's spin and orientation, and the question of whether the transponder would survive the deflection collision of the impactor spacecraft. We propose an alternate scenario in which the orbiting or hovering spacecraft would be tracked from the Earth through standard radiometric methods while the spacecraft in turn images the asteroid to provide its position and velocity relative to the asteroid (Figure 25). The Earth-based radiometric data are Doppler and range, which measure the radial velocity and position, respectively, of the spacecraft with respect to the tracking station, and Delta Differential One-way Range (DDOR), which measures the angular location of the spacecraft relative to two tracking stations. The key to this methodology is the imaging data taken from the spacecraft from which landmark locations on the asteroid could be measured to determine the spacecraft's position relative to the asteroid with fairly high accuracy. This capability was demonstrated on the Japanese Hayabusa mission (Kominato et al., 2006; Gaskell

May contain Caltech/JPL proprietary information and be subject to export control; comply with all applicable U.S. export regulations.

et al., 2006). Further numerical experiments have shown that, with reasonable assumptions about the camera and the ability to perform the landmark detection, the accuracy of the asteroid orbit determination would be nearly identical to that possible using a surface transponder, and might even be better if occultation effects of a landed transponder are considered.

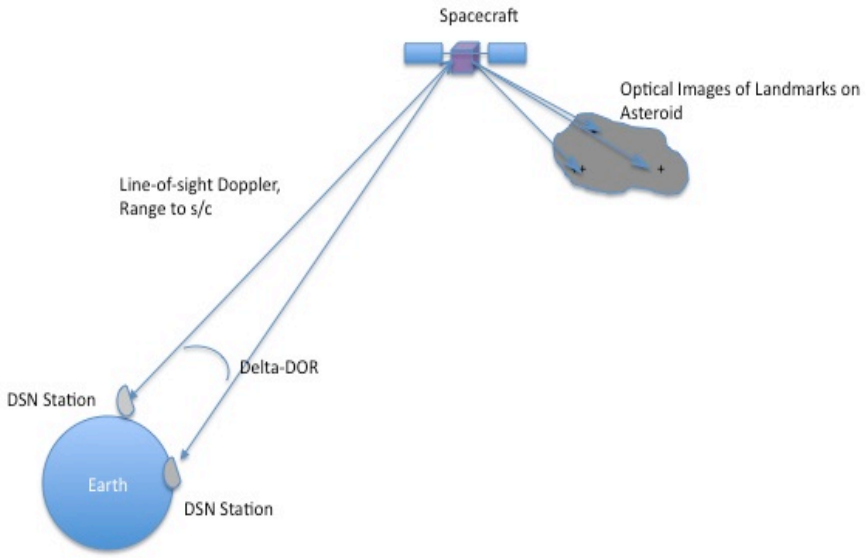

Figure 25: Schematic of data types

Procedure

In order to address the above questions, a covariance analysis was performed to quantify the uncertainties in the asteroid orbit in all the phases. The covariance analysis included the following steps:

1. Numerically integrate a spacecraft trajectory hovering around the asteroid from January 5, 2028 (arrival of the orbiter) to August 4, 2028 (a month after the impact). The control of the spacecraft is not addressed in this study, but other studies, as well as the results from Subtask 2 in this report show that it would be feasible to maintain a pre-defined location near the asteroid. For this covariance analysis, we assumed the spacecraft was in a hovering position roughly 10-15 km from the asteroid's center, in a location perpendicular to the sun line. The results that will be presented, however, are largely independent of the particular hovering location.

May contain Caltech/JPL proprietary information and be subject to export control; comply with all applicable U.S. export regulations.

2. Simulate Doppler and range tracking data at a reasonable frequency during the time span. In principle, the spacecraft could be tracked continuously for the entire time period using the three DSN tracking complexes around the globe. In practice, however, conflicts from other spacecraft would preclude this level of support. For this study, we assumed a background schedule of 3 DSN tracks per week over the entire time span. The Doppler data were weighted at 0.1 mm/s, and the range at 2 m.
3. Simulate DDOR data at a reasonable frequency over the time span. DDOR data require a nearby quasar to track, as well as simultaneous viewing from two DSN complexes. For the quasars, we simulated fictitious quasar locations near the geocentric direction of the asteroid during the tracking phase. The DDOR data were scheduled during Goldstone/Canberra and Goldstone/Madrid overlaps at a rate of two baseline pairs per week. The DDOR data were weighed at a value of 2 nsec.
4. Simulate optical tracking data by scattering landmarks across the asteroid at some reasonable spacing, and take optical measurements of these landmarks at some reasonable frequency. For the landmarks, we assumed a spherical shape (for simplicity) of the asteroid with a diameter of 140 m, and placed landmarks at an equal spacing of roughly 10 degrees over the entire surface. Images of the asteroid were taken at a rate of one per week, except for the period from two weeks prior to impact to four weeks after impact, during which images were taken at a rate of four per day. We assumed an onboard CCD camera with a focal length of 500 mm and a chip size of 1024 square pixels, which gives a total field-of-view (FOV) of 1.4 deg. For any given picture, only landmarks that were in the camera FOV and illuminated by the sun were used in the filter. The optical data were weighted at a value of 0.25 pixels.
5. Set up an estimation filter to process combinations of all three data types, with appropriate weights on the data and a priori uncertainties on the filter parameters. Table 6 lists the complete set of filter parameters and their settings that were used for this analysis. Note that the parameters are divided into the "estimated" and "consider" categories; the "estimated" parameters are ones that are adjusted in the filter, and whose *a priori* uncertainties are therefore reduced as the data are processed, while the "consider" parameters are those which are too weak to be estimated, but whose errors contribute to the final covariance. The output of the filter is a post-fit covariance matrix which provides uncertainties on the spacecraft orbit, asteroid orbit, and ancillary parameters in the filter. The quantity of primary interest is the uncertainty in the asteroid orbit, which is provided as a fully correlated covariance on the Cartesian asteroid state at an epoch time, and this could then be mapped to different coordinate frames and times, such as the time of the 2049 impact. All uncertainty results in this subtask are quoted as 1-sigma values.

May contain Caltech/JPL proprietary information and be subject to export control; comply with all applicable U.S. export regulations.

Table 6. Estimated and considered parameters.

Estimated Parameters	**A priori Uncertainty (1 sigma)**	**Comment**
Position (3 components)	10^6 km	
Velocity (3 components)	10^3 km/s	
Asteroid GM	2.1 x 10^{-9} km^3/s^2	
Asteroid Ephemeris	Correlated covariance	The asteroid's ephemeris is provided as corrections to orbital elements
Bias acceleration (3 components)	10^{-12} km/s^2	Accounts for mismodeling in solar radiation pressure, and errors in small thrusting events
Spacecraft impulsive maneuvers (3 components)	1 mm/s	Accounts for orbit maintenance
Asteroid delta-V (3 components	1 cm/s	
Station range bias	10 m	White noise, per station and pass
Consider Parameters		
DSN station locations	Correlated covariance	Standard set used by navigation teams
Troposphere calibration	10 cm dry, 40 cm wet	
Ionosphere calibration	55 cm day, 15 cm night	
Pole orientation	7.5 nrad	
UT1	0.3 msec	

1.4.4 Subtask 3 Results

The first set of results concerns the 6-month period of time from the orbiter spacecraft arrival in January 2028 through the kinetic deflection in July, 2028. During this time, the spacecraft would be in a stable hovering position near the asteroid and could commence taking optical images of the landmarks while it is simultaneously tracked using Earth-based radiometric data. Prior to this time, the knowledge of the asteroid's orbit would have been obtained solely from Earth-based optical images taken of the asteroid over a period of many years. The primary question to be answered is the level of improvement that could be obtained from these in situ spacecraft measurements. The results are presented in two forms; first in the six classical orbital elements of the asteroid, and then in terms of the major and minor axis of the uncertainty ellipse after mapping the uncertainties to the b-plane of the 2049 encounter with the Earth.

May contain Caltech/JPL proprietary information and be subject to export control; comply with all applicable U.S. export regulations.

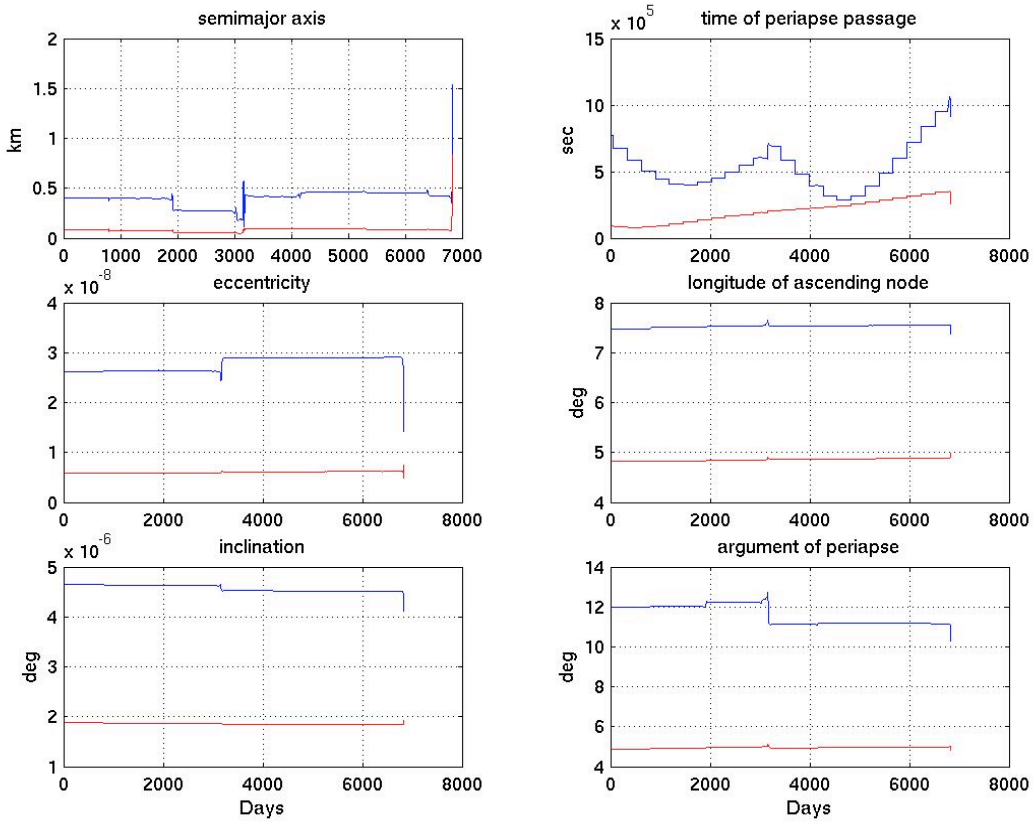

Figure 26. A priori 1-sigma uncertainties in orbital elements (blue lines) and the improved uncertainties (red lines) due to 6 months of tracking prior to the arrival of the kinetic impactor in July 2028.

Figure 26 shows plots of the 1-sigma asteroid ephemeris uncertainties in the 6 classical asteroid orbital elements as functions of time in days after arrival on January 5, 2028 and ending just prior to the close Earth encounter on September 13, 2046. In each plot, the blue line represents the *a priori* knowledge of the asteroid's orbit (i.e., without tracking the orbiter spacecraft), while the red line shows the uncertainties after 6 months of tracking are included. The sudden changes past day 3000 are caused by the distant Earth flyby on August 2036, but the net effect on the uncertainties is only slight. It can be seen that the ground-based ephemeris knowledge is quite good; for example, the semi-major axis has an uncertainty of only 500 m. The results are not mapped beyond the 2046 encounter because this Earth flyby has a large dispersing effect on the uncertainties. This can be seen more clearly in Figures 27 and 28, which

May contain Caltech/JPL proprietary information and be subject to export control; comply with all applicable U.S. export regulations.

plot the asteroid error ellipse uncertainties at the time of the 2046 Earth flyby and the 2049 impact, in their respective b-planes. The horizontal axis in this case represents the number of days of tracking starting on January 5, 2028. Thus, at time 0, no spacecraft tracking has been obtained and the values represent the *a priori* knowledge. Here, it can be seen that at the 2046 flyby, the error ellipse is only 9 x 3.5 km, while in 2049, the major axis has grown considerably so that the ellipse has dimensions of about 800 x 3.5 km.

Next, the radiometric and optical tracking data are added to see how they improve the asteroid ephemeris uncertainty. In Figures 27 and 28, the result is shown as a function of the number of days of tracking for the 2046 and 2049 Earth b-planes, respectively. After 8 days, the impact major axis ellipse has been reduced to about 400 km for the 2049 epoch (the effect of this amount of tracking on the orbital elements is plotted by the red line in Figure 26, which shows a factor of 2-4 improvement in these parameters). Beyond this point, adding more data doesn't result in further improvement, probably due to the presence of the consider parameters and the fact that the asteroid orbit is already well determined. Consider parameters are those that are not solved for within the orbit solution but whose uncertainties do affect the solution uncertainties. Various numerical experiments with different assumptions on the filter parameters indicate that the 8-10 day period appears to be an inflection point where the majority of improvement using the *in situ* data has been reached, at least for this asteroid and time period.

The next step is to examine how well the orbit of the asteroid could be re-determined after the impact on July 4, 2028. It is assumed that the impact would deliver a nominal ΔV to the asteroid of 4.7 mm/s. However, the uncertainty on this value might be large since the blowback momentum is poorly known. Thus, in the covariance analysis, the asteroid ephemeris is assumed to have an applied impulsive ΔV of 4.7 mm/s with an uncertainty of 1 cm/s. This effectively corrupts the ground-based knowledge such that the b-plane uncertainty ellipse semi-major axis at the time of the 2046 and 2049 encounters increases to about 2,000 and 200,000 km, respectively (the semi-minor axis shows little change).

It would take several years to pin down the new asteroid orbit after the deflection if only Earth-based observations were used, as the change to the asteroid's orbit would be relatively small, but *in situ* measurements provide a very powerful way of determining the post-impact orbit. This is seen in Figure 29, which shows the effect on the 2046 and 2049 encounter b-plane uncertainty ellipses of the post-deflection tracking. After only one day of tracking, the semi major axes have been reduced from 2,000 and 200,000 km to roughly 6 and 510 km. Further tracking doesn't have much effect for the next couple of weeks until after about 21 days, when the results improve to values of about 3 km and 125 km, which seems to represent the best that could be done for this time period. It is not entirely clear why, at this time period, the asteroid's orbit could be determined to this level of accuracy whereas in January, the floor value was about 400 km, but it is likely that the relative viewing geometries of the Earth and the asteroid play a major role.

The final objective of this task is to determine the level of accuracy that the asteroid's orbit could be determined following gravity tractoring. The tractoring phase was set to be 200 days long beginning on July 2, 2032 and ending on January 20, 2033. Because this is long after the

May contain Caltech/JPL proprietary information and be subject to export control; comply with all applicable U.S. export regulations.

original tracking period in 2028, and to simplify the set up for the analysis, we reverted to the original ground based *a priori* covariance of the asteroid as a starting point. We then added a transverse acceleration uncertainty to the asteroid during the tracking phase of 2.5×10^{-12} m/sec^2. Unlike in the case of the instantaneous deflection, the net effect on the Earth b-plane uncertainties in 2049 from this disturbance is negligible because of its relatively small magnitude. Thus, at the beginning of the post-tractor phase tracking period on January 20, 2033, the b-plane uncertainty ellipse in 2049 is 800 km, as before.

Figure 30 plots the results of the radiometric and optical tracking of the spacecraft following tractoring. Here, it can be seen that only one day of tracking is needed to bring the uncertainties down to floor values of 3.1 and 260 km for each of the Earth encounters. Adding more tracking has little effect, and it appears that the limit of knowledge has been reached.

Subtask 3 Conclusions

The specific conclusions of this subtask for the scenario analyzed are:

- The asteroid's pre-impact trajectory was determined to a value of about 400 km in the semi major axis of the b-plane uncertainty ellipse at the Earth encounter in 2049. This level is reached after only eight days of tracking the spacecraft once it arrives at the asteroid.

- Following deflection, the asteroid's orbit was determined to its pre-impact levels after only one day of tracking. The ellipse semi-major axis was determined to an accuracy of 125 km after three weeks of tracking (1-sigma).

- Following the tractoring in early 2033, the asteroid's orbit was determined to its pre-tractoring levels again after only one day of tracking. The ellipse semi-major axis knowledge reached a floor value of about 260 km (1 sigma).

Several general conclusions can also be drawn from this study:

- The combination of radiometric tracking of an orbiting or hovering spacecraft with optical imaging of the asteroid from the spacecraft is sufficient to dramatically improve the knowledge of an asteroid's orbit. No transponder on the surface of the asteroid is needed.

- Tracking the asteroid via the spacecraft improves the orbit accuracy by a factor of from 2 to 5 over the accuracy that can be obtained from Earth-based observations of the asteroid. The size of the improvement is dependent on the relative viewing geometry, and hence the time period over which the spacecraft is tracked.

- The length of time it takes to realize improvements in the knowledge of the asteroid's ephemeris is measured in days to weeks. A spacecraft need not be in place for months or years for significant orbit knowledge improvements to take place.

May contain Caltech/JPL proprietary information and be subject to export control; comply with all applicable U.S. export regulations.

- A close flyby, such as the one that occurs in 2046 for this scenario, magnifies uncertainties by a large factor for subsequent flybys.

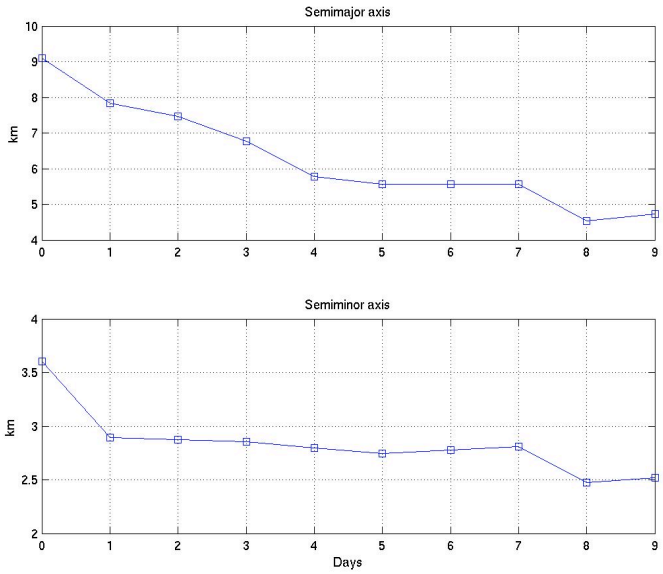

Figure 27: Asteroid uncertainties mapped to the Earth b-plane in September 2046 as a function of the number of tracking days (pre-

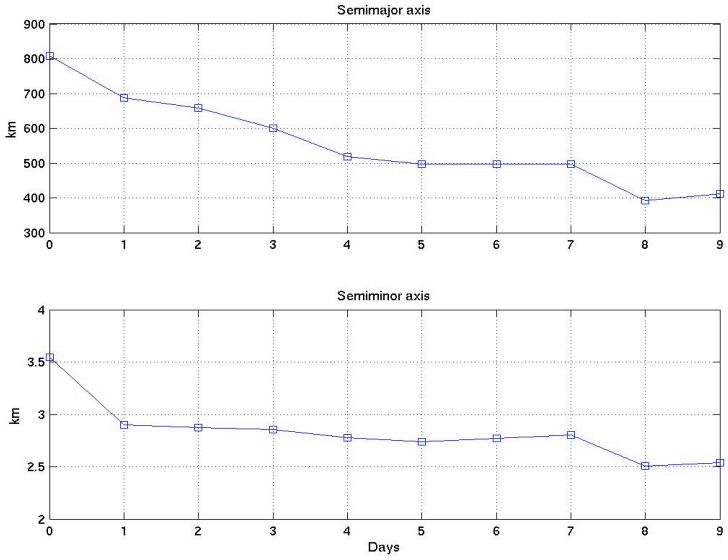

May contain Caltech/JPL proprietary information and be subject to export control; comply with all applicable U.S. export regulations.

Figure 28: Asteroid uncertainties mapped to the Earth b-plane in September 2049 as a function of the number of tracking days (pre-deflection impact).

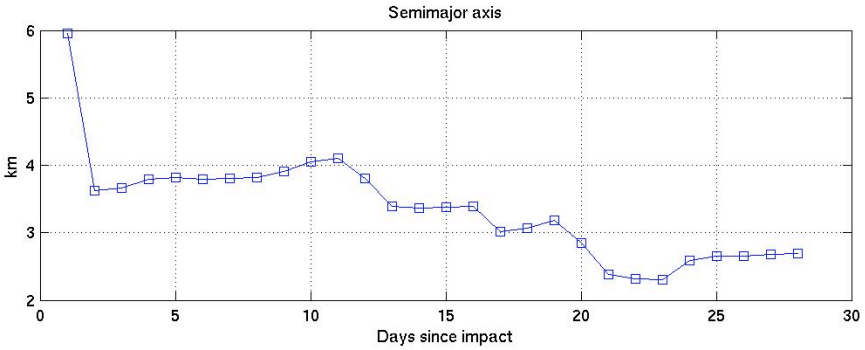

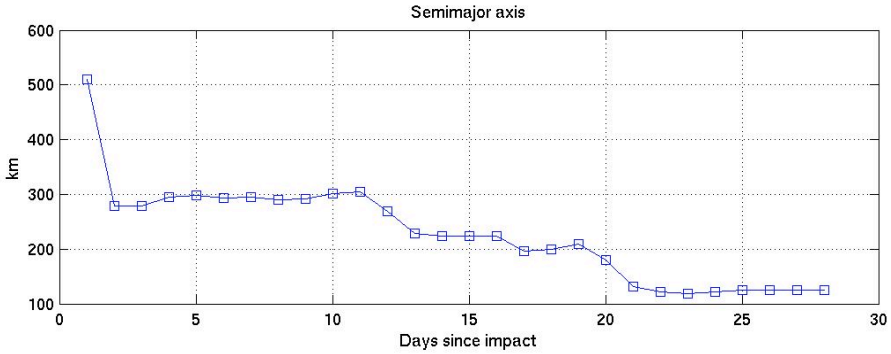

Figure 29: Asteroid uncertainties mapped to the Earth b-plane in September 2046 (top) and September 2049 (bottom) following deflection, as a function of the number of tracking days (post-deflection impact).

May contain Caltech/JPL proprietary information and be subject to export control; comply with all applicable U.S. export regulations.

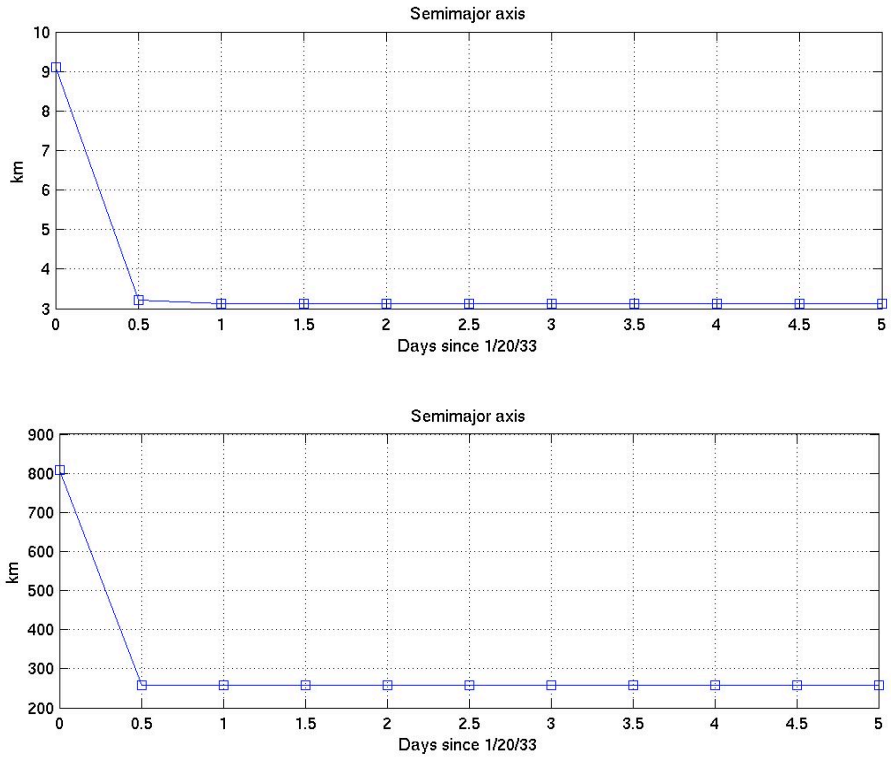

Figure 30: Asteroid uncertainties mapped to the Earth b-plane in September 2046 (top) and September 2049 (bottom) following tractoring as a function of the number of tracking days.

Subtask 4: Preliminary Planning for Analysis of Mission Design and Implementation.

This subtask was to develop a preliminary assessment and set of requirements for the t-GT NEO mission. The results would provide a preliminary scoping of the mission and provide requirements that would be addressed during the Team X study. It would include a pre-session with the Team X leader to develop the necessary documentation of the customer specifications for the NEO mission and reach agreement on Team X study products. The specific tasks are:

1. Develop Level 1 requirements for the t-GT mission.
2. Identify, where possible, existing S/C that would roughly match parameters from Subtask 2 above.
3. Provide a cost by analogous mission of the gravity tractor mission including launch vehicle, based upon Subtask 2 parameters. Provide an annual operations cost (for scaling purposes). Assume a mission could launch to the NEO and use optimal launch and arrival times (i.e., could launch anytime in next 20 years, as opposed to non-optimal launch/ arrival combinations associated with "little warning time to impact" scenarios).

May contain Caltech/JPL proprietary information and be subject to export control; comply with all applicable U.S. export regulations.

1.4.5 Subtask 4 Results

Work on Subtask 4 was descoped as it directly related to preparing for a Team X session. The customer did not express interest in holding a Team X session in the near future.

Analysis of Mission Design and Implementation

Subtask 5: Team X study to develop full mission concept design and cost estimate.

The options outlined in subtask 5 focus upon demonstrating a viable mission and spacecraft design. The options outline conducting an Advanced Project Design Team (Team X) study to develop a rough full mission concept and cost estimate. The two options presented here describe both a full concept study with a cost estimate and a minimal study that outlines a full mission concept with no cost estimate. The work outlined in this subtask, specifically options 1 and 2, are additional services that the customer can select if desired. While results from subtasks 1-4 do not depend upon results from options in subtask 5, pursuing an option in subtask 5 provides mission and spacecraft design details that would enhance the credibility of the concept significantly. If feasibility can be established by doing the groundwork in subtasks 1-3, viable mission and spacecraft design concepts could be achieved by having Team X develop an end-to-end mission design for a t-GT mission consisting of visuals such as the spacecraft configuration, details on each of the spacecraft subsystems including propulsion, as well as a cost estimate based upon the specifics of the mission designed by the team (only for option 1). Work in subtask 5 will be completed by Team X and will be scheduled near the end of the study period so that technical information gained by results from any or all of subtasks 1-4 can be fed directly into the Team X study if the customer selects the baseline or basic option in subtask 5 (see proposal for description of options.

1.4.6 Subtask 5 Results

Should the B612 Foundation decide to award Subtask 5 at later date, JPL will at that time submit a formal Space Act Agreement Revision and Cost Estimate for those activities that will be performed by JPL subject to NASA approval.

1.4.7 Key Milestones and Products

The subtasks (1-4) outlined in the statement of work were initially to take place over 5 work months from the initiation of the contract, February through June. However, delivery of the final report was delayed due to preparation of this material for the Asteroid, Comets, and Meteors Conference in mid-July. The customer agreed to a final report due date of September 1, 2008 at the June 23, 2008 face-to-face meeting held at JPL.

May contain Caltech/JPL proprietary information and be subject to export control; comply with all applicable U.S. export regulations.

1.5 *Study Conclusions*

1. This study has shown that a relatively simple and robust thrust control law can keep a gravity tractor spacecraft in close proximity to the station-keeping location required to effectively tow an irregularly shaped, rotating near-Earth asteroid. For our test case, the spacecraft could be kept within a 20 x 50 x 50 meter box at a nominal distance of 155 meters from the asteroid's center-of-mass for a total translational ΔV monthly cost of 40 - 45 m/s with a corresponding monthly fuel consumption of only ~ 1.4 kg.
2. This modest fuel consumption suggests that for a mission with similar requirements to our baseline, SEP propulsion may not be required; chemical options may be sufficient.
3. About 48% of the expended ΔV was used to pull the asteroid (this was the gravity tractor efficiency).
4. For our simulated test case, where the tractoring spacecraft was about 1000 kg, the total ΔV imparted to the asteroid in one month was about 7 μm/s.
5. The furthest extension of the rotating NEA was ~117 meters.
6. The 2049 impact probability was essentially at 100% prior to the time of the t-GT spacecraft arrival in 2026.
7. The asteroid's pre-deflection trajectory was determined to a 1-sigma value of about 400 km in the semi-major axis of the b-plane uncertainty ellipse at the Earth encounter in 2049. This level was reached after only eight days of tracking the spacecraft once it arrived at the asteroid in 2028. This indicates that the 2049 Earth impact location can be predicted with comparable precision.
8. A 140-m sized, coherent NEA could be deflected from an Earth impact via a 1150 kg kinetic impactor striking the NEA in 2028, some 21 years in advance of the potential Earth impact in 2049.
9. A 4.00 mm/s ΔV in 2028 produced an asteroid deflection of 80,000 km in 2049, more than enough to prevent impact, but a 4.69 mm/s ΔV in 2028 would move the asteroid trajectory into the 6:5 keyhole for a subsequent impact in 2054. Our simulations assumed that the rendezvous spacecraft (t-GT) would be used as a gravity tractor to tow the asteroid an amount sufficient to miss this keyhole in 2049.
10. Following the kinetic impact deflection, the asteroid's orbit was determined to its pre-impact levels after only one day of tracking. The ellipse semi-major axis in the 2049 impact plane was determined to an accuracy of 125 km after three weeks of tracking in 2028.
11. Following the completion of tractoring in early 2033, the asteroid's orbit was determined to its pre-tractoring accuracy levels after only one day of tracking. The uncertainty ellipse semi-major axis knowledge in 2049 reached a floor value of about 260 km (1 sigma).
12. In 200 days of tractoring, starting in mid-2032, the asteroid's uncertainty region could be moved completely off the keyhole with 650 km/260 km = 2.5 sigma level of confidence. This corresponds to an upper bound for the impact probability of 2%. Tractoring could be continued after the 200 days to reach higher confidence levels of avoiding the keyhole. For example, simple scaling indicates that one year of tractoring should effectively clear the keyhole at the 4.6 sigma confidence level (impact probability less than10^{-5}).

May contain Caltech/JPL proprietary information and be subject to export control; comply with all applicable U.S. export regulations.

13. The 6:5 keyhole in 2049 is only 6 km wide and the other six keyholes are similarly narrow, and the likelihood of a passage through any of the keyholes is only ~ 0.02%. But, due to fairly large uncertainties in the asteroid's 2049 ephemeris positions (~260 km, 1-sigma) even after the spacecraft tracking that would follow the July 2028 impactor, the likelihood of having to worry about a keyhole passage is ~100 times larger, or a few percent.
14. Because of intervening approaches to Earth and Venus, the dynamics of our test case was very non-linear and the optimal time for tractoring is not as soon as possible after confirmation that passage through the 6:5 resonant return keyhole is possible. The optimal time for tractoring would be around 2037 when 200 days of tractoring provides ~1500 km motion on the 2049 impact plane – more than enough to ensure the NEA's 3σ uncertainty ellipse would be moved off the relatively tiny keyhole. Other impactor cases, however, could be very different.
15. The one lunar distance encounter in 2046, three years prior to the primary impact in 2049, serves to amplify any deflections obtained before that time, but similarly amplifies the mapped uncertainty. The net effect of the close approach is modest: the gravity tractor can achieve the necessary deflection even without that close approach.
16. A gravity tractor could be useful for the possible case in which a primary deflection technique such as a kinetic impactor happens to move the asteroid trajectory into a keyhole; the gravity tractor could shift the asteroid's trajectory enough to miss a secondary impact keyhole. At the same time, tracking of the gravity tractor spacecraft could provide precision orbit information for the asteroid before and after the primary deflection attempt and after the gravity tractor trim maneuver.
17. While the gravity tractor in our simulation example was a viable method for towing the asteroid away from the 2049 keyhole, and hence avoiding a 2054 Earth collision, there might be other impacting scenarios for which it would not be viable. Each threat scenario would have to be analyzed individually to determine whether a gravity tractor could be used to move an asteroid trajectory away from a keyhole.

Additional general study conclusions include the following:

- The most threatening NEAs are those on Earth similar orbits.
- Simulations show that most actual Earth impactor discoveries surpass 99% impact probability very early in the second optical apparition – or after optical and radar data are obtained during the discovery apparition.
- The primary deflection techniques (e.g., kinetic energy impactor) provide relatively uncertain amounts of deflection (e.g., the momentum multiplier β is unknown)
- Secondary impact possibilities (keyholes) must be carefully examined for each specific case.
- Determining potential keyholes during Earth encounters and determining optimal times for tractoring to avoid a keyhole passage requires fully perturbed, non-linear numerical analysis (two-body analyses do not suffice).

May contain Caltech/JPL proprietary information and be subject to export control; comply with all applicable U.S. export regulations.

- The combination of radiometric tracking of a nearby spacecraft with optical imaging of the asteroid from the spacecraft is sufficient to significantly improve knowledge of an asteroid's orbit. It is not necessary to place a transponder on the surface of the asteroid to achieve precise asteroid tracking.
- The asteroid orbit accuracy improvements provided by the spacecraft range from factors of 2 to 5 over the knowledge which can be obtained using only Earth-based observations of the asteroid. The size of the improvement is dependent on the relative viewing geometry and hence the time period over which the spacecraft is tracked.
- The amount of time it takes to realize these improvements in the knowledge of the asteroid's ephemeris is measured in days to weeks. A spacecraft need not be in place for months or years for the improvements to take place.
- A close flyby, such as the one that occurs in 2046 for this scenario can magnify the asteroid's position uncertainty for subsequent flybys by a large factor.

May contain Caltech/JPL proprietary information and be subject to export control; comply with all applicable U.S. export regulations.

2 References

Broschart, S.B., and D.J. Scheeres (2005), "Control of Hovering Spacecraft near Small-Bodies: Application to Asteroid 25143 Itokawa", *Journal of Guidance, Control, and Dynamics*, Vol.28, No. 2, pp. 343-354.

Broschart, S.B., and D.J. Scheeres (2007), "On the Implementation of Spacecraft Hovering under Reduced-order Dead-band Control", paper presented at the 2007 AAS/AIAA Astrodynamics Specialists Meeting, Mackinaw Island, MI, August 2007, AAS Paper 07-397.

Chesley, S., and P. Chodas (2008), "Gravity Tractor Study Target Selection", memo to the Gravity Tractor Study team, March 7, 2008.

Dawn spacecraft website (2008), http://dawn.jpl.nasa.gov/mission/ion_prop.asp, retrieved on August 26, 2008.

R. Gaskell, O. Barnoin-Jha, D. Scheeres, T. Mukai, N. Hirata, S. Abe, J. Saito, M. Ishiguro, T. Kubota, T. Hashimoto, J. Kawaguchi, M. Yoshikawa, K. Shirakawa, T. Kominato, "Landmark Navigation Studies and Target Characterization in the Hayabusa Encounter with Itokawa", paper presented at the 2006 AAS/AIAA Astrodynamics Specialist Conference, Keystone, CO, August 2006, AAS Paper 06-6660.

Kominato, T., M. Matsuoka, M. Uo, T. Hashimoto, and J. Kawaguchi (2006), "Optical Hybrid Navigation in Hayabusa – Approach, Station Keeping & Hovering", presented at the AAS/AIAA Spaceflight Mechanics Meeting, Tampa, Florida, January 22-26, AAS Paper 06-209.

Lu, E.T., and S.G. Love (2005), "A Gravitational Tractor for Towing Asteroids", *Nature,* Vol. 438, No. 2., pp. 177-178.

Ostro, S.J., L.A.M. Benner, C. Magri, J.D. Giorgini, R. Rose, R.F. Jurgens, D.K. Yeomans, A.A. Hine, M.C. Nolan, D.J. Scheeres, S.B. Broschart, M. Kaasalainen, and J. Margot (2005), "Radar Observations of Itokawa in 2004 and improved shape estimation", *Meteoritics and Planetary Science*, Vol. 40, No. 11, pp. 1563-1574.

Scheeres, D.J., and F. Marzari (2002), "Spacecraft Dynamics in the Vicinity of a Comet", *Journal of the Astronautical Sciences*, Vol. 50, No. 1, pp. 35-52.

Werner, R.A., and D.J. Scheeres (1997), "Exterior Gravitation of a Polyhedron Derived and Compared with Harmonic and Mascon Gravitation Representations of Asteroid 4769 Castalia," Celestial Mechanics and Dynamical Astronomy Vol 65, pp.313-44.

May contain Caltech/JPL proprietary information and be subject to export control; comply with all applicable U.S. export regulations.

Valsecchi , G.B., A. Milani, G.F. Gronchi, S.R. Chesley.(2003). "Resonant Returns to Close Approaches: Analytic Theory." *Astronomy and Astrophysics*, Vol408, pp. 1179-1196.

May contain Caltech/JPL proprietary information and be subject to export control; comply with all applicable U.S. export regulations.